The Thesis Committee for John J Borer IV
Certifies that this is the approved version of the following thesis:

Mobile Robot Operator for Downstream Oil & Gas Industrial Facilities

APPROVED BY

SUPERVISING COMMITTEE:

Eric van Oort, Supervisor

Mitchell Pryor

Mobile Robot Operator for Downstream Oil & Gas Industrial Facilities

by

John J Borer IV

THESIS

Presented to the Faculty of the Graduate School of

The University of Texas at Austin

in Partial Fulfillment

of the Requirements

for the Degree of

MASTER OF SCIENCE IN ENGINEERING

THE UNIVERSITY OF TEXAS AT AUSTIN

December 2020

Dedication

Dedicated to my Mom and Dad, siblings, and three great groups of friends in New Jersey, Oklahoma, and Texas.

Acknowledgments

My good friends Brian, Josh, Damian, Cicio, Welbon, Aditya, Son, and Motaz made my two years in Austin amazing. Thank you to my family for being as supportive as any family could be and always making me feel welcome back home.

I cannot thank Dr. Pryor enough for making my graduate experience so enjoyable and productive. Thank you to Phillips 66 for sponsoring this work and providing guidance throughout its course.

Abstract

Mobile Robot Operator for Downstream Oil & Gas Industrial Facilities

John J Borer IV, M.S.E.
The University of Texas at Austin, 2020

Supervisor: Eric van Oort

This thesis considers the application of robots in downstream Oil & Gas facilities. Automation is important in industrial facilities where improvements in safety, efficiency, and environmental performance are becoming increasingly important. Here we present a mobile robotic platform for the performance of inspection and survey tasks in downstream facilities. We demonstrate a hybrid localization strategy using a novel metric which allows for long term autonomy in large distributed industrial environments. An environmental sensing package and gas source localization algorithm are deployed on the platform to identify and localize fugitive emission sources. Our mobile robotic platform, hybrid localization strategy, and gas source localization algorithm form an autonomous remote operator capable of meaningfully contributing to the advancement of automation in industrial facilities.

Table of Contents

List of Figures

Chapter 1

Introduction

This work examines and demonstrates the use of robotic systems for autonomous localization and survey in downstream oil and gas (O&G) processing facilities. System operators in O&G and similar facilities face hazards including poisonous or explosive gasses, pressurized containers, and fall hazards. Demonstrating the capability of a mobile platform to automate a subset of routine inspection tasks that expose operators to these hazards is the goal of this work. Capabilities demonstrated here can be applied across a wide variety of industrial sites and domains.

1.1 The Need for Robots in Oil and Gas Facilities

Oil and gas processing operations take place across a broad range of industrial sites including refineries, pipeline terminals, and tank farms. Each facility serves a unique function but share in common a general hazard profile associated with their role as processors of pressurized, flammable, and volatile liquids. Immensely complex suites of industrial machinery which need continuous monitoring and inspection are required to safely handle these hydrocarbon products. Containing pressurized liquid or gas within myriad different pipes, valves, tanks, and pumps, some of considerable age, is a challenging task. Among such a complex system there is the potential for

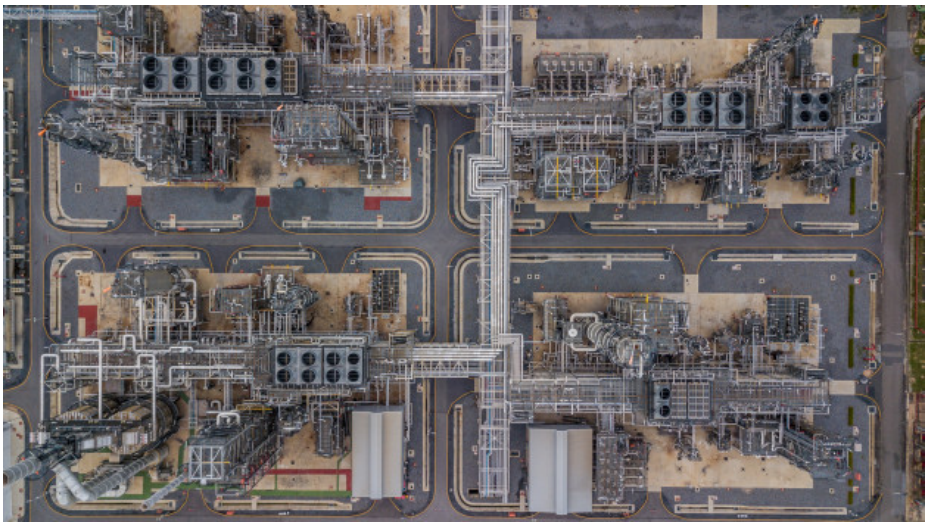

Figure 1.1: Example refinery environment showing the complex integrated nature of a hydrocarbon processing facility. Note how the individual process blocks are crowded but separated by large open spaces. [13]

leakage and emission into the atmosphere of some portion of the processed volume.

These fugitive emissions are undesirable and their detection is the focus of routine inspection tasks. Static sensing arrays are able to detect fugitive emissions, but are prone to false alarm, and their cost and complexity limit the number that can be installed on any one location. Human operators with handheld gas sniffers are required to inspect emission hot spots when a static sensor signals a detection event. A mobile robotic platform mounted with gas sensing equipment can perform this same task without exposing humans to risk. In addition to fugitive emission sensing, robotic platforms can be used to inspect valves and pressure gauges, audio emissions, and safety conditions. Robotic labor augmentation allows the human operator to perform tasks that take advantage of their critical thinking and creativity while eliminating dull and dangerous routine duties.

Furthermore, robotic platforms bring with them powerful computational capabilities. In addition to sensing, algorithms can process and examine many data streams to provide the operator data to better understand facility state. This data and analysis can be recorded and stored with perfect fidelity for future use in a unified information processing workflow. These capabilities avoid many of the errors encountered by humans performing repetitive tasks under stress during which they are expected to record and analyze data.

There are however downsides of robotic platforms. They lack critical reasoning, handle environmental dynamism poorly, and are constrained in their ability to physically access the world. These downsides, along with numerous others not listed here, generally mean that robotics platforms are well placed to augment operators but not replace them. There is a readily identifiable subset of tasks that robotic systems excel at, but until facilities and workflows are made to accommodate automated inspection systems, they will remain a tool in the tool box at the disposal of plant operators.

1.2 Problem Definition

Our goal, to automate oil and gas facility fugitive emission survey tasks, is comprised of two distinct parts. Part one is providing a system capable of performing mobile patrols of a large processing facility. Part two is identifying and applying algorithms to solve the fugitive emission source localization problem. This structure mimics the role operators currently perform and builds new capabilities by taking advantage of the tools a mobile robotic platform has.

An array of technology, software, and hardware are required to effectively solve both of these tasks. Our work draws on existing solutions to aspects of the problem including robot navigation and localization, obstacle avoidance, and plume modeling. We then expand from these foundations applying new capabilities and structure. This work seeks to demonstrate an extensible framework for robotics in industrial environments and show the applicability of the open source Robot Operating System (ROS) for future research and deployment applications. Our goal of providing solutions within the ROS environment influenced technical decisions and software design.

Autonomous navigation in large structured environments like oil and gas processing centers is challenging. Dynamic obstacles including vehicles and humans require active local planning and object avoidance. In addition to dynamic obstacles, the intricate 3D structure of process blocks makes characterizing the overhead space a requirement for path planning.

Navigating across a large facility with areas of obstructed overhead view poses two distinct problems. First, the facility is too large and and too dynamic to make generating a comprehensive static map for localization feasible. Second, overhead obstruction blocks Global Navigation Satellite Systems (GNSS) in large parts of the facility which make localization and path planning with GNSS alone impossible. This context can be visualized in Fig. 1.1 where large open spaces in between process blocks, and crowded spaces within process blocks complement each other. We refer to this context, of being unable to depend solely on a static map or GNSS for localization, as hybrid localization. It is the hybrid localization problem which we solve by building

and improving upon previously existing methods. Provided with the ability to localize in hybrid environments and avoid obstacles during navigation, mimicking facility operator inspection rounds is feasible.

Here we present a novel, metric based on GNSS carrier noise, re-initialization framework to manage transitions between localization modalities which accounts for the loss of sensor data needed by specific localization algorithms. The algorithm presented here is evaluated in a real-world environment and demonstrated on a mobile robotic platform localizing in an area characterized by regions that favor different localization modalities where the regions are generally known and consistent over time.

If static fugitive emission sensors in a processing facility alarm, personnel are required to confirm the conditions which the alarm signals actually exist. Intermittent leaks and calibration issues often cause false alarms which expend valuable operator resources during inspections. The platform's primary goal is the verification of static emission sensor alarms. However during inspection tasks it can take advantage of its environmental sensing package to provide a detailed characterization of the source state to repair crews.

Accurately characterizing the dispersion of gaseous wind born pollutants like fugitive hydrocarbon emissions from mobile robotic platforms is a challenging and open problem. Wind models depend on large measurement sets and are described by a large parameter space required to characterize the stochastic nature of fluid flow. Additionally emission source rates may vary over time as processing pressures fluctuate and machinery is actuated. Finally, sensors required to effectively capture

the measurement needed to describe the emission source state are limited in their accuracy, solution time convergence, and coverage.

Our robot platform carries wind and gas sensors to provide the environmental sensing capability required to evaluate emission localization models. The stochastic nature of the transport and emission phenomenon, and our inability to guarantee solution convexity in complex environments encourages the use of Monte Carlo Bayesian methods for source localization. We present an application of particle filtering using the platforms sensing suite in concert with a Gaussian Plume (GP) transport model to predict fugitive emission source state. This capability, instead of mimicking a previously performed task, introduces a new capability and meaningfully enhances the facility operator's ability to locate and diagnose problem emission areas.

1.2.1 Hybrid Global Localization Problem

Our mobile platform's pose can be represented in a coordinate space with n poses $\mathcal{P} = \{P_1, P_2, \ldots, P_n\}$. For the general case, localization is performed in six dimensional space, but for our case assuming a level working area, this reduces to two linear dimensions and one angular dimension in $\mathbb{R}^3$. Each pose $P_i \in \mathbb{R}^3$ can be represented as (x_i, y_i, θ_i). Where x_i and y_i are position and θ_i orientation. Continuously providing an estimate of this 2D pose in sensor occluded environments is the responsibility of a hybrid localization algorithm.

1.2.2 Gas Emission Source Localization Problem

Fugitive emissions sources are considered as point sources with a fixed emission rate. For the general case consider the $\mathbb{R}^4$ space with s sources $\mathcal{S} = \{S_1, S_2, \ldots, S_s\}$. Each source $S_i \in \mathbb{R}^4$ is represented as (x_i, y_i, z_i, q_i) where x_i, y_i, z_i is the source position and q_i the source emission rate. While our research group has previously studied multisource problems related to radiation here we consider only a single source S with state invariant with respect to time.

The mobile platform as it traverses the facility work space produces m measurements $\mathcal{M} = \{M_1, M_2, \ldots, M_m\}$. Each measurement M_i is a tuple $(W_i, c_i, t_i, x_i, y_i, z_i)$ where the first term is a wind measurement, the second term a gas concentration, the third a time stamp, and the final three a map location. Each wind measurement W_i is composed of the wind velocity v_i and wind azimuth ϕ_i. The concentration measurement is used directly in the source localization algorithm and the wind measurement is used to parameterize the emission forward transport model. Note that the emission sensor used is considered to not be directionally dependent. Thus for gas source localization, the pose of the robot for purposes of placing the sensor (as opposed to hybrid localization) further reduces to $\mathbb{R}^2$ inclusive of (x_i, y_i).

1.3 Summary of Objectives

This thesis provides an understanding of the fully equipped mobile platform "Philbart", algorithms deployed on it, and its application in an O&G facility. Robots in industrial facilities performing patrol and sensing have proliferated. Improvements in and reduction in cost of sensing hardware like LIDAR, gas and wind sensors, and

GNSS receivers has made long term multi-purpose autonomy possible.

Here we present the two main areas considered in this thesis; contributions to localization for long-term autonomy and gas source localization. First, an algorithm for maintaining an accurate estimate of the robots pose P_{robot} with two intermittently available localization modes. Second, an application for predicting the state of a single fugitive emission source S given a set of measurements $\mathcal{M}$ automatically collected around the work space. Specifically the material covered here includes,

- Describe the Philbart mobile robot platform and how it is equipped to operate in an industrial facility
- Understand hybrid localization and how it deployed in the field
- Examine the how hybrid localization performed during a robot deployment on the University of Texas campus
- Review gas source localization and its implementation
- Show the effectiveness of our proposed gas source localization algorithm in simulation.

We describe and demonstrate a field deployable mobile robotic platform platform ready to advance the state of the art in downstream O&G facility automation.

1.4 Organization

First, we review work already done in the three previously discussed focus areas; applied robotics in O&G facilities, localization in the presence of sensor occlusions, and gas source localization. All three areas are highly active areas of research and industrial development. Relevant preexisting efforts are discussed in the literature review.

A commercial platform and sensor suite were selected early in the timeline and are described in Chapter Three. The literature review explains why this is possible as multiple hardware options have proven feasible to meet the domain and task requirements. It is their autonomous capabilities that must be improved. Thus Chapter Three reviews the Philbart robotic platform, its sensor payload, and summarizes key design choices. A key requirement for the hardware selection was compatibility with ROS through open interfaces or existing drivers. By using ROS, we can building on existing software middleware and packages which dramatically reduce the software engineering effort and assure the system can be developed in the future. In this chapter, we discuss how ROS accelerated our development process and how it can accelerate the deployment of robotic platforms in O&G facilities across the application spectrum.

Chapters Four and Five go into detail on the hybrid localization and gas source localization algorithms. Providing the requisite background information to understand their deployment, design, and mathematical background. A background in Bayesian statistics is helpful to fully understand the material. Each chapter presents the results of experiments testing the respective algorithm. The original intention

was to deploy and test the Philbart platform at a decommissioned processing facility in Oklahoma. Unfortunately however the 2020 Corona Virus pandemic prevented this from coming to fruition in time for this work. Instead we present the results of hybrid localization on the University Of Texas campus and gas source localization in a simulated olfactory sensing environment. Chapter six presents conclusions and speculates on how further work can contiue to explore the application of mobile robotics in industrial facilities.

Chapter 2

Literature Review

Here we review published literature that addresses industrial automation in O&G, hybrid localization, and gas source localization. Automation in O&G, including mobile robots, is a relatively new area and focuses primarily on high cost offshore upstream applications. With the advent of cheaper hardware and more robust software, automated systems are beginning to make their way into all parts of the ecosystem.

Hybrid localization technology is an area of active and fast-paced research with huge implications for the future of autonomous vehicles. There is an established corpus of material covering a broad range of applications, here we will explore some of these areas to provide the context to understand our design choice. Emission source localization has a long history tightly aligned with the progression of the environmental movement, and here we will focus on its adaptation to mobile robots. Our platform's objective is primarily gas source detection with a secondary goal of localization. For this reason, we approach the task differently than many proposed solutions where source localization is the primary task.

2.1 Robotics in Oil & Gas

There are a variety of efforts deploying robots or remote systems in refinery or related industrial settings. Here we focus only on those few systems that would meet the necessary specification related to our objectives or include features worth noting relating to their autonomous capabilities that could support the objectives above.

In 2009, Fraunhofer Institute for Manufacturing Engineering and Automation in collaboration with the University of Stuggart deployed one of the first robots in an O&G processing facility [27]. Researchers deployed the MIMROex mobile robot (Fig. 2.1) on an active offshore processing platform. Tasks such as visual inspection and navigation were taught to the platform with a teach pendant and then executed autonomously. A reflective landmark based localization scheme required modifying the operating environment and created a burden on the operators tasked with deploying and maintaining the system. During testing on an operational offshore production facility MIMROex spent 50% of its time conducting reflective landmark mapping, a considerable time sink. Operating the robot in potentially explosive atmospheres required ATEX certification [2] which extended development time and limited hardware choices. For platforms intended to validate robot application in example industrial O&G facilities the certification requirement is onerous and not necessary if an analog environment can be produced.

Shell in coordination with Carnegie Mellon University developed the Sensabot mobile robot (Fig. 2.2) in two design iterations, Mark 1 deployed in 2011, and Mark 2 deployed in 2015 [62]. The platform was designed for deployment in the North Caspian on remotely operated production facilities in the Kashagan oil megaproject.

Figure 2.1: MIMROex deployed on an offshore production facility inspecting a component. [11]

Early in the design phase teleoperation was identified as the target operation mode in order to build trust with skeptical plant operators and managers. The platform is equipped with gas, noise, visual, and vibration sensors to assess plant operating conditions. Mark 2 is equipped with a manipulator capable of moving or reorienting its sensor payload in the workspace. In order to operate in hazardous environments each component, including more than a dozen custom enclosures, underwent IECEx certification [8]. The platform weighs 450kg and is capable of traversing multi-level processing blocks with the use of custom installed climbing racks.

TOTAL launched the Autonomous Robots for Oil and Gas Sites (ARGOS) challenge in 2013 [47]. Two applications were identified as the focus of the effort, the first being emergency operations and the second, routine facility inspection. Dual use robots are valuable because platforms meant solely for emergency response are

Figure 2.2: Sensabot Mark2 with boom mounted sensing payload for deployment in hard to reach areas. The cog rail system gears, for multi-level traversal, are mounted externally on the wheel hubs. [16]

used rarely and are difficult to integrate with operation teams. Team ARGONAUTS (Fig. 2.3), a collaboration between Taurob and TU Darmstadt, won first place [46]. Autonomous behavior was blended with user supervised control to reduce the information load during remote task execution. The open source ROS middleware was used to implement arm motion planning, autonomous mapping, and navigation algorithms. ATEX certification [2], a requirement of the ARGOS challenge, allows the platform to be deployed in classified hazardous environments, but limited widespread unclassified testing and autonomous capability verification.

While some aspects of the tasks were automated, none of the three platforms utilized fully autonomous behavior, and none have been scaled to full widely used

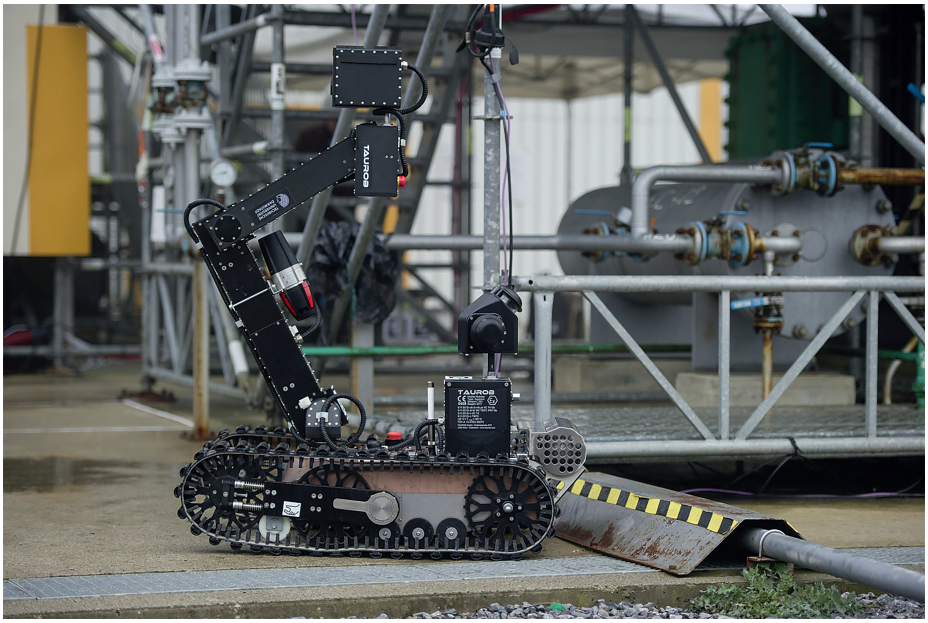

Figure 2.3: Argonaut, the ARGOS challenge winning platform deployed for testing in Total's Shetland gas plan. [1]

commercial applications.

Recently commercial hazardous atmosphere certified platforms have come to market. ExRobotics [3] has deployed over 20 remote operator platforms in O&G facilities across the globe. However they have limited autonomous capabilities, for example localization and navigation tasks are controlled by following a stripe of orange tape placed on the ground. Furthermore operators have run into roadblocks servicing the certified platforms at their own facilities when mechanical problems surface.

2.2 Hybrid Localization

Accurate and continuous estimation of a mobile robotic platform's pose is a requirement for long-term autonomy. The proliferation of inexpensive sensor technology and reliable open source software has facilitated the introduction of mobile platforms into university campuses, industrial facilities, and transportation networks. This project, in part, harnesses this technology and deploys it in downstream O&G facilities. A common sensor suite for these platforms typically consists of a combination of wheel encoders, an inertial measurement unit (IMU), stereo cameras, a LIDAR, and a Global Navigation Satellite System (GNSS) receiver. Combined, they enable a variety of sensor fusion filtering techniques used to generate a state estimate of the robot's pose. Each sensor has strengths which our proposed hybrid localization algorithm takes advantage of so that a sensor is always available to produce an accurate pose estimate.

Wheel encoders have the desirable property of measuring wheel motion regardless of external disturbance. When used to estimate robot pose however, slippage and the lack of an external reference means that the uncertainty in the state estimate grows without bound. Therefore a system cannot depend solely on wheel encoders, but they are useful for estimates over short periods of time when no externally referenced pose measurement is available.

LIDAR and GNSS produce data that can be used to generate an externally referenced pose estimate with bounded error. Environmental characteristics such as large feature-free areas, overhead obstructions, and indoor/outdoor spaces interfere with the ability of either to continuously generate reliable information. Environ-

mentally specific sensor-dependent occlusion degrades the ability of mobile robot platforms using these sensors to track their position in commonly encountered application domains.

In a large and complex real-world facility such as an industrial facility, sensor occlusions can be caused by many environmental factors:

- Variation in the ground surface due to surface type, weather, etc.
- Including both indoor and outdoor regions of interest
- Communication lapses including WIFI, cellular, GNSS, or radio due to physical occlusion
- Local interference with sensors due glare, electromagnetic interference, etc.

Robotic platforms must maintain a valid pose estimate while considering the inevitable failure of sensors used to determine its pose.

2.2.1 Technologies

Optimal estimation of the change in pose of an outdoor mobile robot while receiving intermittent GNSS solution data has been previously examined in [33] [64] [67] [38]. Fusing accurate wheel encoder odometry with available GNSS measurements allows for continuous state estimation in the event of GNSS occlusions. Once GNSS has been lost however the state estimate uncertainty, conditioned only on wheel encoder odometry, grows without bound until a usable GNSS signal is reacquired. These methods are predicated on the notion that GNSS coverage will be reacquired before

Figure 2.4: Differential drive autonomous ground vehicle robotic operator Philbart with LIDAR and GNSS receivers.

the state estimate degrades beyond a usability threshold. For applications where a total GNSS blackout occurs for extended periods or wheel odometry degrades rapidly, this is not the case.

Autonomous vehicles operating in urban spaces with degraded GNSS coverage are an area of active research interest. Image-based localization [72] [74] is popular for its low hardware cost and high reliability when accurately initialized. However it depends on robust pre-execution environmental characterization which can be costly and time prohibitive. Furthermore it requires conditions favorable for imaging that are impossible to guarantee and can be effected by lighting, weather conditions, and

proximity.

Simultaneous Localization and Mapping (SLAM) of large urban spaces with GNSS drift correction [50] [69] is a proven way to generate large scale maps as input for probabilistic localization algorithms like Monte Carlo Localization (MCL). In large obstacle free areas, even if the map is accurately generated, will not be useful for LIDAR based probabilistic localization algorithms. These techniques require extensive data management and may fail in dynamic environments such as industrial facilities. Without dedicated data acquisition hardware and software pipelines this solution can be unwieldy, over paramaterized, and not easily maintained.

Opportunistic sensing takes advantage of widely proliferated wireless networks [30] - of particular interest due to forthcoming 5G infrastructure - and can provide robust continuous localization solutions for urban spaces where these signals proliferate. This however is predicated on the presence of the relevant networks and the availability of appropriate sensor technologies, and neither may be available in remote facilities where robotics can be most useful. Also high frequency signals that are used by opportunistic sensing localization are easily degraded by physical obstructions like those commonly found in industrial facilities.

Researchers [22] [24] have directly integrated GNSS measurements into existing LIDAR based MCL algorithms. The contribution from each pose estimate data source (GNSS or MCL) is weighted by the relative information contained in each. This method is also predicated on the ability to generate and manage continuous maps across large spaces which as previously mentioned is a challenging task for large industrial facilities.

Both [71] [32] consider transitioning between LIDAR and GNSS based localization in structured hybrid environments. Partitioning the work-space into discrete LIDAR or GNSS available zones provides an intuitive way to understand and manage localization needs and thus limit the requirement for large and difficult to maintain maps. Decisions to transition between localization modes are made based on either GNSS position covariance or the operator's learned experience. Without an informed metric that accurately reflects sensor occlusion, switching between localization modalities is a manual and error prone process.

Structured transition between LIDAR and GNSS localization based on sensor availability is an efficient and effective way to maintain accurate hybrid localization. Methods that require full facility maps which are difficult to acquire and maintain are not practical for facilities without dedicated technical staff. Nor is opportunistic sensing, which depends on signals which often are not present, a viable solution. Here we propose a solution that addresses the problem of identifying the best localization modality given a dynamic, sensor occluding environment.

2.3 Source Localization

Transport modeling and source localization has previously been demonstrated in the literature, approaches to both are discussed here.

2.3.1 Source Localization in Other Disciplines

A diverse set of technical disciplines have an interest in locating a source using measurements of the effect the source has on the environment. This general

class of problems often has both optimization and Bayesian based solutions. For the case of linear problems, linear optimization techniques or linear Bayesian methods like Kalman filters are optimal. Non-linear domains are addressed with non-linear optimization or non-linear Bayesian methods.

The electroencephalogram (EEG) is a technique to measure neuron activity in the brain. Identifying the activity source center using noisy measurements and an imperfect source model is a localization problem analogous to our own. He [37] showed non-linear optimization under simplifying constraints produced a solution which best explained the measurement in a norm squared error sense. Antelis [25] proposed both Kalman and Particle filters to solve the same problem in the Bayesian framework. Bayesian methods have the benefit of producing a most likely estimate and covariance which quantifies the certainty of the estimate. Work in EEG neuron activity source localization is challenged by the specification of representative source models which can be used to accurately predict measurements. Specifying an accurate source and transport model is also an important and challenging part of the gas source localization problem.

Nuclear facilities can contain large amounts of hazardous nuclear material. During processing, storing, or transporting the material radiation can be accidentally released. Locating the source of errant radiation emissions is a task regularly performed by radiation control technicians (RCT). During this survey process the RCT may be exposed to radiation which is undesirable for their health and safety, and facility operation. Howse [40] used an array of four stationary detectors to track the position of a moving source using a non-linear least squares estimator. This problem

formulation closely mimics our gas source localization model except that in our case there is a single sensor that is moved to multiple locations via a robot and the source itself is stationary. Anderson [48] applied a particle filter to localize stationary radiation sources using a mobile measurement robot, in an approach directly analogous to our own. The method developed by Anderson *et al.* allow for different transport models to be used within the algorithm. In general, radiation localization benefits from a more structured source model which describes how radiation intensity attenuates as the inverse squared distance. However when physical attenuation is taken into account model complexity grows and the problem is challenging to solve for the general case.

2.3.2 Gaussian Plume Transport Model

Efforts to understand the flow of pollutants in advective and diffusive flow began as early as the 1920's. It was realized early that ensemble averaged concentration profiles of an emission source undergoing advective and diffusive dispersal had structure [49]. The GP model produces analytical forecasts of atmospheric dispersion of wind borne pollutants by describing this ensemble averaged concentration profile. It combines the estimates from Turner's Workbook of Atmospheric Dispersion Estimates [70] with meteorological data to calculate a 2D Gaussian shaped profile of dispersion as a function of atmospheric stability and downwind distance.

Intended to calculate the impact of emissions from industrial emission sources, the model and its derivatives has found widespread acceptance by US regulatory bodies [23]. Commonly evaluated at downwind distances of 0.5-100km and over extended

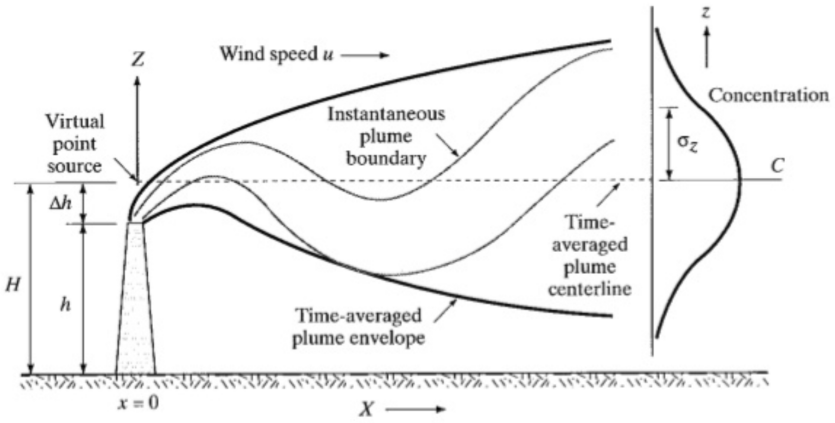

Figure 2.5: Graphical depiction of the GP model. Note the model captures the ensemble average of the oscillating instantaneous plume boundary, and that dispersion σ increases as a function of downwind distance X. [5]

time spans, it has been shown to accurately model the dispersion of non-buoyant emissions. The GP model was not originally intended to predict hectometer scale dispersion on short time scales. In particular Pasquill's [61] stability classes, commonly used to parameterize the model, describe atmospheric characteristics on a regional level and multi-hour/day time scale. Regardless of intention, the model has been used as a transport model of choice for gas dispersion estimation at a variety of scales due to its simple parametrization, computational tractability, and relative accuracy [41]. In chapter 5 we will examine the model more closely.

2.3.3 Filament Dispersion Model

Introduced in 2002 [31], the filament model describes dispersion in turbulent fluid. It bridges the gap between complete discretized numerical simulation and time

averaged ensemble averaging like the GP model.

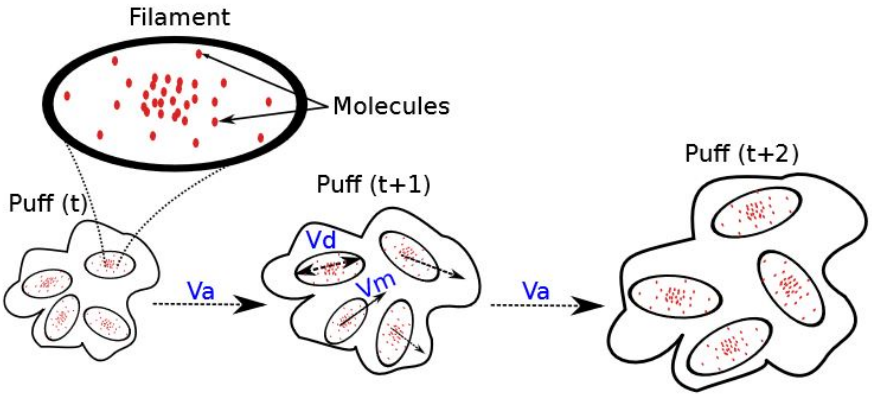

Figure 2.6: The filament dispersion model. Puffs released by the emission source are composed of filaments modeled as collections of molecules. As time progresses the puffs disperse due to turbulent effects. [4]

Chemical releases are represented as a series of puffs. Each puff is composed of a number of filaments where each filament is modeled as a cloud of particles whose distribution is described by a 3D Gaussian. See Fig. 2.6 for a graphical depiction of the abstraction. The model considers that point source chemical releases are manipulated by three phenomenon,

1. Turbulent Diffusion
2. Molecular Diffusion
3. Wind Driven Advection

Diffusion drives dispersion whereas advection drives transport. The relative length scale of the turbulence, referred to as eddy scale, effects how the turbulent

diffusion effects the dispersion process. Molecular diffusion has a relatively small impact on the macro scale when compared to turbulent diffusion and wind driven advection. The three commonly considered turbulent diffusion scales and their effects are given in decreasing eddy scale as:

1. Eddies larger than each puff transport the puff as a whole- these cause a sinusoidal pattern that when time averaged resembles the GP
2. Eddies on the same scale as a puff- greatly distorts each individual puff by displacing filaments from the center axis
3. Eddies smaller than each puff locally mix the particles- this causes little change to the macroscopic behavior of the plume

The filament model is used to validate our implementation of the source localization algorithm in a simulated environment.

2.3.4 Source Characterization Using Static Sensor Arrays

Middleton [57] applied the GP model to predict the concentration of nitrogen oxides near an elevated freeway interchange. Modeling the freeway as a discretized set of point sources produced a downwind concentration profile that agreed well with ground truth measurements taken on a sub-kilometer scale. With the validated model, they predicted the effect of freeway elevation on the downwind dispersal of highway pollution on nearby residential areas.

Bourque [29] used a Lagrangian puff model, which when averaged over time approximates the GP model, to evaluate the deposition of sulfur dioxide downwind of an elevated industrial emission stack. The Lagrangian puff model uses an auto-correlated time scale dependent parameter and accounts for scale dependent wind speed variation to model the dispersal of wind blown pollutants. Measurements acquired with a truck mounted sulfur dioxide sensor driven across the plume and 29 static sulfation plates validated the model's dispersal prediction's over the downwind region. Combining mobile and static sensors is a paradigm that can be applied to O&G facilities where static gas sensing networks may already exist and can therefore be augmented with the introduction of mobile sensing platforms like Philbart.

Hosseini [39] presents a Bayesian framework using the GP forward model to estimate the source emission rate of particulate matter from an industrial lead smelting facility. Before data collection, the estimated emission regions were identified and their centroids calculated. This reduced the state space of the solution to strictly the multi-source emission rates. Particulate emission was estimated from seven distinct zones, using measurements from downwind active and dust-jar accumulation sensors. Although difficult to validate, the estimated source terms correlated well with the relative activity in each emission zone.

The three cases shown above are predicated on a known emission source location. Given a known source location, the source state space is limited to a single variable describing the emission rate. Our case considers an unknown source location and emission rate. The the application of the forward model is the same in both cases regardless of the state size. Optimization and Bayesian methods which evaluate

both the source emission rate and location provide more information. Without an informative prior on the emission location as is the case for our deployment scenario in large O&G facilities, estimating both terms is required, and is the problem solved in our implementation.

Optimization is a method to find the minimum cost of an objective function. This requires an initial guess for the source term and a set of measurements that can be evaluated against model predictions. Pattern search, a gradient free optimization technique, was used in [75] to estimate the complete source term of a single source using the GP transport model. It is highly dependent on initialization, but converges faster than direct gradient methods when initialized properly. Genetic algorithms, which can avoid the local optima pitfalls of gradient and pattern search methods, have also been explored. Haupt [36] demonstrated the potential of a genetic algorithm to solve the global optimization source localization problem, including the wind parameter state, using the GP forward model.

Bayesian methods, instead of producing a single optimal solution, generate a probability density over the state space. Source term estimation is the process of finding the emission rate and location that create the most peaked probability density function in the state space. Although Bayesian methods explicitly account for noise in the sensor, transport, and source model, accurately calculating these noise terms is challenging and an understood limitation. Due to transport model and measurement model non-linearity, Monte Carlo methods that directly sample the probability distribution are commonly used [41]. Samples of the state space allow for direct forward calculation of the transport model which ensures that the probability

distribution is accurately transformed and unconstrained by the limitations imposed by probability distribution models.

Markov Chain Monte Carlo (MCMC) methods construct an ensemble of Markov chains colloquially referred to as "walkers", each representing a sample of the state space. The integral of the walkers at any time step can be used to analytically reconstruct the probability density function at that point. Auto-correlated noise is added to each sample, and states which are more likely, are more often accepted for inclusion. After a convergence period the sampled distribution reaches a steady state which represents the underlying state distribution.

Keats [45] used the adjoint of the transport equation with MCMC sampling to estimate the mean and quantify the uncertainty of a source release in an urban environment. Use of the adjoint eliminated repeated forward transport model evaluations, and by preserving computer power, allowed for more dense MCMC sampling of the state space. This yielded a tractable solution capable of accurately calculating the source term for an emission source in an urban area. Even when not explicitly accounting for the complex urban environment perturbing wind pattern, the method returned an informative estimate of both the state and uncertainty. Other's [43] [65] [73] expand on the use of MCMC methods for GSL. These include different proposal distribution generation methods, sample inclusion heuristics, and multiple sources respectively.

Sequential Monte Carlo (SMC) methods represent the state space with a discrete weighted set of samples. Instead of storing an entire history of belief, from which auto-correlated noise is generated from, each generation of samples is considered in-

dependently. Efficiently and accurately drawing samples from the prior distribution then weighting them proportional to the measurement likelihood, will produce a progressively more accurate estimate of the source term as measurements are taken. Gunatilaka [35] presented an SMC method to estimate the source parameters of a chemical plume source in a simulated environment. Importance sampling was used to iteratively generate more samples in areas of the state space that contribute more to the probability distribution. Progressive Correction was used to extract information from sparse priors more quickly, which decreased convergence time.

Both Li [51] and Neumann [60] combine SMC with sequential importance resampling on mobile robot platforms to localize an outdoor gas source in real experiments. The use of mobile sensors allowed for the integration of informative search strategies, discussed here in the next section. A challenge faced by SMC methods is an inability to accurately quantify the uncertainty in the transport and measurement model, which leads to spurious estimate uncertainty. With testing and calibrating these noise parameters can be tuned or automatically learned. Our implementation uses a SMC method, also called a particle filter, to solve the GSL problem. It uses importance sampling and resampling to avoid degeneracy and maintain a full coverage of the relevant state space.

2.3.5 Source Characterization Using Mobile Sensors

Development of increasingly sensitive sensors and compact low power electronic packaging has made possible the use of fully mobile gas sensors on vehicles, robots, and drones. These technological advances combined with an increase in do-

mestic natural gas productions and sharpened focus on environmental stewardship have increased interest in optimal planning for gas emission survey platforms. In addition to traditional *in-situ* sensors, remote sensors like infrared cameras can also be used to localize emissions sources from a distance [26]. This sensing paradigm is not considered here because it is out of the application project scope and cannot be effectively applied when GSL is a secondary system objective.

Source seeking algorithms have been deployed on mobile robotic gas sensing platforms, drones, and ground vehicles. Researchers have sought inspiration from *taxis*-the movement of an organism in response to external stimuli. The response to chemical stimuli like food, called *chemotaxis*, is a gradient based searched method found widely in the biological world. Its effective application by terrestrial animals sparked interest in the robotics community [55] [54]. There are however shortcomings with chemotaxis, like the underlying assumption that concentration continuously increases close to the source. Complex wind dynamics often rule this assumption null and variation in wind direction during sensing can meaningfully impact its ability to converge. Furthermore the ability of the platform to physically approach the emission source cannot be guaranteed in an O&G processing facility. Also, the source may be intermittent and temporally dependent on process activities. Finally, because gas source localization is a secondary task of the platform considered here, physical source localization behaviors like chemotaxis which require the directed motion of the platform cannot be performed while executing the primary task.

Motion in response to fluid flow, *anemotaxis*, like wind or water is another widely found biological source seeking behavior that has found interest in the GSL

robotics community. Algorithms that mimic this behavior as found in nature like plume crossing upwind search [42] take advantage of both chemical and wind sensors. This dual dependency can makes them more robust to low wind speeds and intermittent gas sensor readings. However the methods are predicated on the notion that gas sources are upwind and that almost full facility coverage is available, which often is not the case.

Mobile robotic gas sensing research focuses primarily on optimal search strategies. Taking account for chemical gradients *chemotaxis*, fluid flow *anemotaxis*, or information gain *infotaxis*. By and large the source term estimation algorithms, if deployed, are the same as those applied with static sensor networks. Mobile systems however benefit from more complete sensor coverage and the ability to optimize measurement location, which can yield faster converging and more precise source term estimates.

2.4 Summary

Mobile robotic systems have been deployed across a variety of O&G production and processing facilities. The documented efforts shown focused on building a certified platform for deployment in real hazardous environments. These systems prove that systems can be certified, but at what cost. What is now needed is improvements in their *value* as tools in a hazardous facility that is sufficient to justify the certification expense. Informed by the difficulty and expense taken to deploy a certified system, our approach is the opposite. Deploy a non-certified system to prove the concept and then later when the applications have been proven, consider certified platforms.

Hybrid localization is a widely explored but still open challenge. Considering the deployment environment that our platform is intended for we adopt a rule-based switching strategy. We improve on [71] [32] by introducing a new metric taking advantage of the GNSS carrier noise ratio. We demonstrate that the carrier noise ratio captures the transition between LIDAR and GNSS preferred environments. Gas source localization is a secondary objective of our platform, and therefore a passive, non-source seeking, particle filter localization strategy is used. We apply the GP model in concert with the algorithm from [51], but instead consider a continuous measurement space instead of a boolean space. Then we validate our algorithm against using the filament model [31] in the GADEN simulator [58].

Chapter 3

Experimental Platform

Since the purpose of this research is to develop improved autonomous capabilities instead of certifiable hardware, the project could be completed with an assembly of commercial off the shelf (COTS) robotic hardware and sensors that are compatible with the Robot Operating System ROS. Using COTS systems instead of building a prototype system, allowed the project to accommodate a relatively short development timeline. Both lead-time for delivery and operational capabilities out of the box were key requirements, as was assurances that components could be replaced or bought at scale by the sponsor if the project was successful. For these reasons, this chapter summarizes the hardware and software configuration.

A medium sized differential drive base was chosen as the platform. Computing and sensor hardware was added as required to produce the capabilities needed to serve the functions previously described. The on-board computer runs Linux and the software stack is built around the ROS middleware.

3.1 Hardware

The base is a Clearpath Husky (Fig. 3.1), a widely available research and industrial platform. Its battery system has been upgraded to a 40Ah high density

Lithium Ion pack which can power the robot for four hours. This extended operating window, twice what the lead acid battery provided, is important for operations in large industrial spaces. Considering that the platform will be operating in an outdoor environment the base has been weatherized to an IP55 rating. This means that it is protected against damaging dust ingress and water spray.

Figure 3.1: Clearpath Husky base without external sensor payloads. Large pneumatic tires allow the platform to safely travel across a broad spectrum of surfaces. [7]

3.1.1 Range Sensors

Ranger sensors provide valuable information for localization and obstacle avoidance algorithms. Laser based sensors like LIDAR are accurate over long distances and are useful for mapping and localization. Operating in a complex 3D environment like a refinery however poses additional challenges considering that the 3D structure of

the environment must be considered for obstacle avoidance. Due to the high cost of 3D LIDAR systems the platform has been equipped with a 2D LIDAR and multiple 3D stereo cameras.

LIDAR

A forward facing SICK Tim571 (Fig. 3.2a) is mounted on the front of the top plate. It has maximum range of 25m, an aperture of 270°, and and angular resolution of 0.33°. It is rated for outdoor use and has an IP67 rating. Onboard power is provided by the platform's auxiliary power supply infrastructure. Data is returned to the onboard computer via an ethernet port and fed directly into a ROS enabled driver interface where it is then fed into localization and obstacle avoidance algorithms.

RealSense Stereo Cameras

Four Intel RealSense D435 cameras (Fig. 3.2b) using active infrared stereo vision are mounted on the forward portion of the top plate. Two are forward and two are side facing, which provides robust coverage of the frontal 3D space. Each has a maximum rated range of 10m that in practice depends on lighting conditions. Best performance has been achieved during nighttime or indoor operation where direct sunlight cannot impinge on the sensor. To reduce the volume of data processed and remove noisier more distant measurements the range is artificially reduced to 5m or less. Power is provided to the cameras through a common powered USB3 hub. Data is fed to the onboard computer where it is used for obstacle avoidance.

The capabilities of depth cameras are rapidly improving. Since the time of the purchase new cameras are available using stereo vision with light [21] and ultrasonic [19] sensors.

(a) Sick Tim571 weatherproof 2D LIDAR [17]

(b) Intel RealSense D435 with active infrared stereo RGB-D

Figure 3.2: The two range sensors mounted on Philart, the LIDAR used for Monte Carlo Localization and mapping, and the RealSense used for 3D obstacle avoidance during navigation. [9]

3.1.2 Referenced Position Sensors

Measurement devices that directly capture information about the kinematic state of the platform are critical inputs into localization algorithms. The platform has two earth referenced sensors, both the GNSS and IMU, and one self referenced sensor, the wheel encoders.

Global Navigation Satellite System

GNSS systems produce earth referenced measurements of the platform's latitude and longitude. These are then transformed into a local coordinate system in which the measurement is then converted into the platforms (x, y) location with respect to the deployment area datum.

Two Swift Navigation Duro (Fig. 3.3a) GNSS receivers, each with their own antenna, are mounted on two offset corners of the platform. One receiver calculates position, and the second is referenced to the first to calculate heading. Both solutions vary in quality (i.e. precision and accuracy) considerably depending on satellite coverage and solution correction availability. A real time kinematic (RTK) correction when available allows for the calculation of solutions accurate to less than 2cm. In commonly encountered GNSS occluded environments the coverage is sporadic and must be accommodated by the localization system.

Inertial Measurement Unit

The inertial measurement unit (IMU) measures acceleration, angular position, and angular rate with an accelerometer, magnetometer, and gyroscope respectively. These measurement can be used in an absolute, relative, or integrated manner to generate estimates of the robots kinematic state.

A Lord MicroStrain 3DM-GX5-25 (Fig. 3.3b) mounted on the underside of the top plate feeds this data directly into the onboard computer via USB3 which also provides power to the device. Magnetic interference and high vibration meaningfully impacts the quality of the generated measurement data. Practice has shown

(a) Swift Navigation Duro ruggedized GNSS receiver (bottom) and antenna [18]

(b) Lord Microstrain inertial measurement unit with triaxial accelerometer, gyroscope, and magnetometer [10]

Figure 3.3: Eternally referenced positions sensors on the Philbart platform.

the magnetometer to produce unreliable orientation data and the accelerometer to produce mixed results in real field deployments. This inability to measure an accurate magnetic azimuth influenced our decision to choose a static datum and manual initialization in our hybrid localization algorithm.

Wheel Encoders

Each motor drive assembly, one for each side, has wheel encoders which measure the the angular displacement of the motor at its measurement frequency. Given the wheel radius, this angular velocity can be converted into an estimate of the wheels linear velocity. This velocity can then be integrated to position to provided a position estimate referenced to the point where the platform started counting encoder rotation.

Noise in the measurement device itself, slippage between the driving surface and wheels, and an imperfect turning model reduce the wheel encoder's position

estimate accuracy. Over short distances, 0-25m the information can provide a valuable and continuous position reference, but over greater distances, or after sharp turns the accuracy of the estimate will degrade significantly. For this effort, the weight of the sensors on the system odometry tuning model does not significantly impact the default tuning. In a refinery setting, variation in the ground surface may impact turning and thus it will be critical to validate the system's odometry generated pose with other sensing modalities.

3.1.3 Environmental Sensing

In order to paramaterize the gas source localization transport model and generate measurements for the particle filter the environmental sensing package consisting of an anemometer and gas sensor is used.

Anemometer

The GP transport model, used to predict the downwind concentration of a pollutant, requires the wind speed and direction as input. Under the assumptions applied to the environment for the GP model the values measured on the robot are assumed constant and uniform across the workspace.

Philbart is equipped with a MaxiMet GMX200 2D sonic anemometer capable of measuring wind speed and direction from 0.01m/s to 60 m/s over a 360° azimuth. It generates nearly instantaneous measurements and publishes them at 1Hz to a RS232-USB3 adapter plugged into the onboard USB3 hub. Data is fed into a simple ROS driver node which decodes the serial message and publishes the wind speed and

azimuth as a 2D vector in the anemometer_link frame.

Gas Sensor

To evaluate the likelihood function in the particle filter a measurement of the true gas concentration is needed. Each particles evaluated likelihood is used to weight it according to the probability that it represents the source which produced the true measurement.

A RKI M2A explosion proof Methane sensor is mounted on Philbart's sensor rack. The measured concentration ranges from 0-9000 ppm and is given with a resolution of 20ppm. It's 30 second or less measurement response time means that it does not provide an instantaneous reading, but on the time and space scales that our platform operates at it is fit for the purpose. Both analog amperage and digital outputs are available from the sensor's control computer. Our platform uses the digital 2-wire RS-485 modbus communication protocol which allows Philbart to monitor system state in addition to the measured concentration.

(a) MaxiMet GMX200 2D ultrasonic anemometer [6]

(b) RKI M2A explosion proof infrared gas sensor, configure to detect methane [14]

Figure 3.4: Philbart's environmental sensing package measurements are used to evaluate the gas source localization algorithm.

3.2 Software

The onboard computer runs the Ubuntu 18.04LTS Linux distribution operating system. Open source robotics software is primarily targeted at Linux distributions and provides a level of control that is more challenging to acquire on Windows systems. Furthermore, the robotics community has adopted Linux as the operating system of choice writ large, which means that much of the open source software the platform takes advantage of are poorly supported elsewhere.

In order to manage and control the interaction of all the different parts of the

system the Melodic distribution of ROS is deployed on the computer. It is the most widely distributed and used open source robotic middleware in the world and has solutions to many commonly encountered problems such as visualization, communication, and control. Its system model is a graph structure (Fig. 3.5), where processes are represented as *nodes* and communication between processes are represented as edges called *topics*.

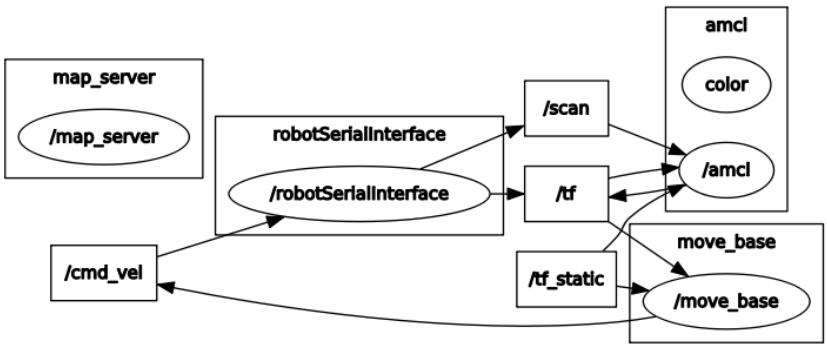

Figure 3.5: Example ROS graph structure. Nodes are represented as ovals inside of their enclosing namespace and topics are represented by rectangles connected with directed arrows to nodes. [15]

This graph structure divides the complex layout of the system into independent pieces with discrete responsibilities and dependencies. In addition to nodes and topics there is also a parameter server, services, and actions which provide additional functionality. Onboard processes, each performed in individual nodes, are broken down into three general categories,

1. Driver Nodes- Run, monitor, and process sensors

2. Utility Nodes- Responsible for hardware control and monitoring system health
3. Function Nodes- Implement high level functionality like navigation, localization, and sensing

This discretized structure, found both in ROS itself and our high level node class abstraction, allows for rapid development, stable software APIs, and reliable operation during development. It is notable that team Argonaut [46], the winner of the ARGOS challenge, also used ROS to on their platform. This allows for energy and time to be focused on testing and application instead of troubleshooting and development.

Chapter 4

Hybrid Localization

State of a mobile vehicle can be represented by its full, 12 member (6DOF) spatial kinematic description:

$$\bar{\mathbf{x}} = [\ X\ \theta\ \dot{X}\ \dot{\theta}\ ]^T \tag{4.1}$$

where $X = [\ x\ y\ z\ ]$ represent the linear dimension and $\theta = [\ \theta_R\ \theta_P\ \theta_Y\ ]$ represent the angular dimension. Dot notation is used to indicate the first derivative with respect to time. Modeling limitations and noise in the process and measurement force us to consider a most likely estimate of the state $\hat{\mathbf{x}}$, instead of the true state $\bar{\mathbf{x}}$.

4.1 Transformation Tree

The Robot Operating System (ROS) guideline for mobile platform coordinate frames [56] establishes a best practice regarding how coordinate transforms should be structured. The *base_link* frame is a robot fixed frame attached at a fixed location on the platform, like the center of the bottom base plate. Each onboard measurement is collected in their respective *sensor_link* frame and transformed to the *base_link* frame.

The *odom* frame is a world fixed frame in which the pose of the robot is refreshed at a high frequency. Estimates generated in the *odom* frame are generally

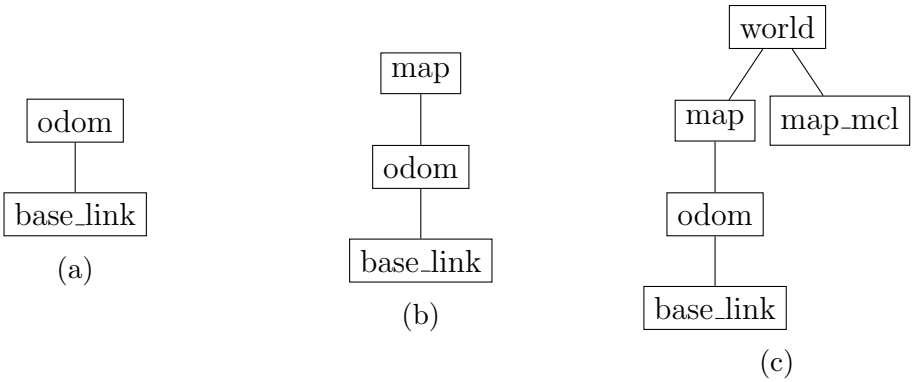

Figure 4.1: Mobile robot transformation trees increasing in the number of externally referenced measurements from left to right.

self-referenced and accumulate error over time. High frequency continuous data like wheel encoder odometry is used to generate the *odom* → *base_link* transform. For our purposes the *odom* frame can serve as a short horizon reference but is not suitable for extended periods of travel, particularly when turning sharply or on loose surfaces.

The *map* is a world fixed frame in which the robot pose error is bounded when measurements are available. Unlike the *odom* frame it is not continuous and can experience instantaneous discrete jumps. Low frequency discrete data like MCL or GNSS pose is used to generate the *map* → *odom* transform. Incorporating globally referenced measurements ensures that the *map* frame can be used as a long-term reference.

When no externally referenced pose measurement is available, a mobile robot's transform tree includes only the *odom* and *base_link* frames (Fig. 4.1a). Given either a GNSS or MCL generated pose measurement, the tree includes all three primary frames (Fig. 4.1b).

4.1.1 Hybrid Localization Transformation Tree

When two externally referenced pose measurement sources are available - as is the case considered here - each sensor's measurement frame is considered individually (Fig 4.1c). Latitude and longitude solutions generated by the GNSS receiver are converted into an (x, y) position measured in meters displaced from a site specific GNSS datum δ_{GNSS}. The datum is itself an earth referenced latitude and longitude coordinate local to the operational area. The MCL pose is generated with respect to an arbitrary *map_mcl* frame whose origin carries no fundamental earth referenced meaning and is a function only of the mapping algorithm used to acquire the map.

Given that the deployment area is large, maps can only be recorded in subspaces of the navigable region. For this reason, the robot's *map* frame was selected to be the the GNSS measurement frame. This means that GNSS solutions can be directly integrated into the estimator and that MCL poses first must be transformed from the arbitrary *map_mcl* frame into the robot's *map* frame. In order to generate this transform the MCL and GNSS reference frames are registered using a least squares optimization on correspondent points measured in both frames.

4.2 Pose Measurement Sources

The following section reviews our pose measurement methods to provide the required background to understand our hybrid localization strategy. In general our method can extend to include any number of globally referenced measurement sources. Here however our method and the measurement heuristic we present are based on the GNSS and LIDAR sensing paradigm available on our platform.

4.2.1 GNSS

Orbiting satellites transmit encoded "navigation messages" towards earth. Each message includes the encoding satellite's coordinate in the geocentric coordinate system WGS-84 and a time generated by an on-board atomic clock. When received by the platform's on-board receiver the time of arrival is recorded. The difference in time between message generation and its arrival is used to calculate the distance between the satellite and receiver given the speed of the transmission media [28].

Given at least four unique satellites, trilateration can be used to calculate the position of the receiver on the earth. Errors associated with the receivers on-board clock mean that the calculated distances, referred to as pseudoranges, potentially have significant error.

Two solution methods, code phase or the much more accurate carrier phase, are used to calculate pseudorange. Code phase measurements depend on the comparison of the pseudorandom code generated between the satellite and receiver. This code generation occurs on the microsecond scale which can introduce +100m error in electromagentic signals traveling at the speed of light. The GNSS signal carrier phase has a frequency of over 1 GHz and serves as a more accurate calibration reference, facilitating the calculation of solutions with sub-centimeter error.

The variance of the four solution types available on our platforms receiver is given in Table 4.1. These values were provided by the GNSS software manufacturer, and then calibrated during real deployment experiments

Table 4.1: Solution Accuracy

Solution Type	***σ (m)***
SPP	25.0
SPP-SBAS	15.0
Float RTK	4.0
Fixed RTK	0.01

[a]Standard deviation is for horizontal position accuracy.

4.2.2 MCL

Monte Carlo localization is a well-established and widely deployed probabilistic localization solution in robotics [68]. It takes advantage of a particle filter's weighted discrete representation of state and ability to accurately capture the effects of non-linearity in the state equations.

For the 2D flat-world case considered here, MCL estimates the pose of the platform given odometry u, a range sensor measurement z and a known map M. Provided an initial state estimate $(x, y, \theta)_0$, an odometry motion model $p(x_i|x_{i-1}, u_i)$, and a measurement likelihood function $p(z_i|x_i, M)$, MCL will iteratively generate a probabilistic pose estimate.

Requiring an initial state estimate distinguishes MCL from GNSS which is a true earth referenced measurement needing only to be acquired and not initialized. Initializing the MCL filter at the proper time is one of the primary tasks for our hybrid localization implementation.

4.2.3 GNSS Carrier Noise

GNSS receiver accuracy depends on generating code and carrier frequency copies that replicate the signal generated by the satellite. If these signals are inaccurately recreated then they cannot be matched to the measured signal. The carrier frequency is more sensitive to signal interference than the code frequency and can be used as an accurate proxy for GNSS solution availability [66].

When the noise is greater than the GNSS receivers tolerance the carrier to noise ratio will drop below its threshold value,

$$\frac{C}{N_0} < \frac{C}{N_{0\,threshold}} \tag{4.2}$$

In this cases the carrier tracking loop will loose the GNSS lock and begin generating spurious noisy solutions. Field testing has shown that this threshold serves as an effective and proactive indicator of GNSS solution availability which can be used to manage localization sensor stream priority.

4.3 State Estimation

Extended Kalman Filter implementations, introduced in the 1960s [44], have been used to estimate state in broad number of application domains. EKF's are able to handle moderate non-linearity while remaining computationally tractable. They do this by linearizing the model about the mean estimate using the Jacobian. Our system's pose can be described by a nonlinear dynamic system,

$$\mathbf{x}_k = f(\mathbf{x}_{k-1}) + \mathbf{w}_{k-1} \tag{4.3}$$

Where $\mathbf{w}_{k-1} \sim \mathcal{N}(0, Q_{k-1})$ and $\mathbf{x}_k$ is our length 12 state vector representing the 6 DOF kinematic description. Measurements $\mathbf{z}_k$ are considered nonlinear functions of the state that are corrupted by zero mean Gaussian measurement noise.

$$\mathbf{z}_k = h(\mathbf{x}_k) + \mathbf{v}_k \tag{4.4}$$

Where $\mathbf{v}_k \sim \mathcal{N}(0, R_k)$ and $\mathbf{h}$ is the measurement transition function. Prediction of the mean and covariance are shown in (4.5) and (4.6) respectively.

$$\hat{\mathbf{x}}_k = \mathbf{f}(\mathbf{x}_{k-1}) \tag{4.5}$$

$$\hat{\mathbf{P}}_k = \mathbf{F}\mathbf{P}_{k-1}\mathbf{F}^T + \mathbf{Q}_{k-1} \tag{4.6}$$

Here f is a 3D omnidirectional motion model derived directly from Newtonian mechanics for a point mass. Evaluating the predicted estimate error covariance (4.6) is accomplished by projecting forward with the transfer function Jacobian $\mathbf{F}$ $\mathbf{f}$ evaluated at the current estimated state $\mathbf{x}_{k-1}$ and corrupting with process noise Q_{k-1}. When a sensor measurement is received, the EKF correction step is executed,

$$\mathbf{S}_k = \mathbf{H}_k\hat{\mathbf{P}}_k\mathbf{H}_k^T + \mathbf{R}_k \tag{4.7}$$

$$\mathbf{K}_k = \hat{\mathbf{P}}_k\mathbf{H}_k^T\mathbf{S}_k^{-1} \tag{4.8}$$

$$\mathbf{x}_k = \hat{\mathbf{x}}_k + \mathbf{K}_k(\mathbf{z}_k - \mathbf{H}_k\hat{\mathbf{x}}_k) \tag{4.9}$$

$$\mathbf{P}_k = (\mathbf{I} - \mathbf{K}_k\mathbf{H}_k)\hat{\mathbf{P}}_k \tag{4.10}$$

First, the innovation covariance $\mathbf{S}_k$ and the semi-optimal Kalman gain $\mathbf{K}_k$ are calculated. Then the corrected mean (4.9) and covariance (4.10) can be calculated in parallel. The Jacobian $\mathbf{H}_k$ of the measurement transition function $\mathbf{h}$ evaluated at the mean is then used to predict the measurement's expected value.

4.3.1 Disturbance Rejection

The generic implementation of the EKF shown above will incorporate all measurements regardless of the likelihood that the measurement was truly produced by observing the state. An errant measurement is one that deviates from the predicted value significantly. These measurements have the potential to meaningfully degrade the quality of the corrected state estimate. Errant measurements can be received by the EKF when the GNSS quality degrades, MCL is not initialized, or when sensors malfunction. Rejecting these measurements ensures that transitions happen smoothly and the estimate maintains its accuracy.

Mahlalanbois distance is a multidimensional generalization of the distance between a point and a distribution (4.11). The inverse weighted squared difference of the true measurement $\mathbf{z}_k$ and the predicted the measurement $\mathbf{H}_k\hat{\mathbf{x}}_k$ quantifies the distance between the sample $\mathbf{z}_k$ and the distribution $\mathcal{N} \sim (\mathbf{H}_k\hat{\mathbf{x}}_k, \mathbf{S}_k)$.

$$\mathbf{d}_M^2(\mathbf{z}_k) = (\mathbf{z}_k - \mathbf{H}_k\hat{\mathbf{x}}_k)^T\mathbf{S}_k^{-1}(\mathbf{z}_k - \mathbf{H}_k\hat{\mathbf{x}}_k) \tag{4.11}$$

For a for a given measurement source specific threshold α_s, a measurement $\mathbf{z}_{sk}$ will be rejected if $\mathbf{d}_{Msk}^2 > \alpha_s^2$ [63]. Effectively this acts as an estimate-uncertainty scaled protection against spurious data.

4.4 Hybrid Localization

Mappable areas and areas with good GNSS coverage are often, but not necessarily, complementary. A hybrid localization framework should be able to maintain a continuous pose estimate in the presence of changing localization modalities. A static

globally referenced coordinate frame to which both GNSS and MCL measurements can be referenced must be established first. This frame should be unambiguous, fixed in the real world, and readily measured with one of the sensing modalities. A GNSS coordinate and East North-Up frame (ENU) fit these criteria and can be readily and repeatably selected with survey tools or available web mapping services. Initialization of the state filter with a logged pose is required on startup. For the intended application of our platform, a mobile survey robot, this reflects the reality of being stored at a single location and repeatedly deployed on a survey route over the course of an operational deployment.

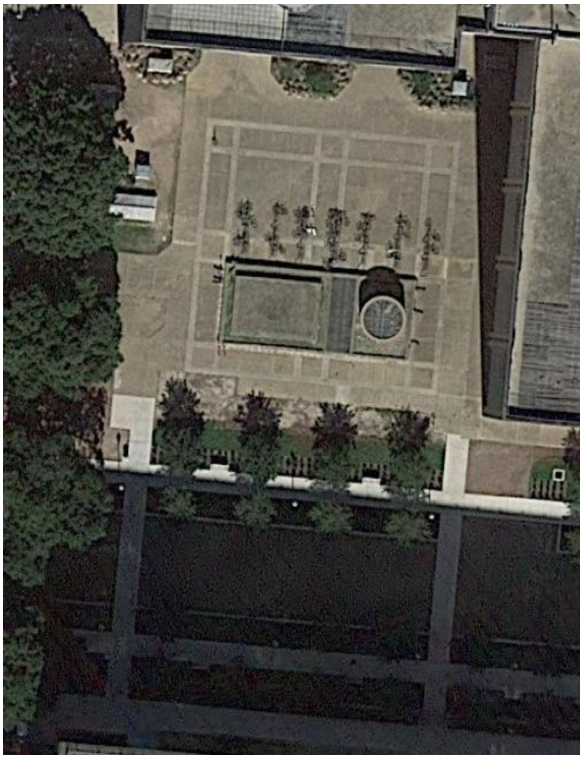

Figure 4.2: Deployment area shown from Google maps. The building in the upper right corner is 19 stories tall. The overall space is approximately 60x60 meters including a large open plaza, treed area, grass, pavement and large air exhaust outlet. [20]

Algorithm 1 details the logic behind measurement availability and filter re-initialization. Algorithm 2 shows our EKF implementation and takes account for disturbance rejection.

Four phases of operation defined by dominant localization modality were considered by [71],

1. GNSS

2. GNSS $\rightarrow$ MCL

3. MCL

4. MCL → GNSS

Where the → indicates that a transition from an area of GNSS coverage to MCL coverage occurs or vice versa. This pattern of GNSS → MCL → GNSS describes common outdoor robotics application areas, particularly in distributed industrial facilities.

Algorithm 1 Hybrid Localization

$\hat{\mathbf{x}} \leftarrow \mathbf{x}_{init}$ {Initialize filter state}
while $True$ **do**
  if $\mathbf{z}_{GNSS}$ **then** {Solution Available}
    $\hat{\mathbf{x}} \leftarrow EKF(\mathbf{z}_{GNSS})$
  end if
  $\hat{\mathbf{x}} \leftarrow EKF(\mathbf{z}_{MCL})$
  if $CN_0 < CN_{0_{lim}}$ **then** {Lost GNSS}
    $\hat{\mathbf{x}}_{MCL} \leftarrow \hat{\mathbf{x}}$ {Reinitialize MCL filter}
  end if
end while

Algorithm 2 EKF w/ Disturbance Rejection

$\hat{\mathbf{x}}_k = \mathbf{f}(\mathbf{x}_{k-1})$
$\hat{\mathbf{P}}_k = \mathbf{F}\mathbf{P}_{k-1}\mathbf{F}^T + \mathbf{Q}_{k-1}$
$\tilde{\mathbf{y}}_{sk} = \mathbf{z}_{sk} - \mathbf{H}_{sk}\hat{\mathbf{x}}_k$
if $\mathbf{d}_M^2(\mathbf{z}_{sk}) < \alpha_s^2$ **then** {Accept measurement}
  $\mathbf{x}_k = \hat{\mathbf{x}}_k + \mathbf{K}_k(\mathbf{z}_k - \mathbf{H}_k\hat{\mathbf{x}}_k)$
  $\mathbf{P}_k = (\mathbf{I} - \mathbf{K}_k\mathbf{H}_k)\hat{\mathbf{P}}_k$
else {Reject measurement}
  continue;
end if

GNSS

During GNSS only operation a low variance solution is available and this measurement will dominate the state estimate. High variance MCL pose estimates, unable to converge because of limited map coverage, will be considered disturbances and rejected by the Mahalanbois threshold α_s. If GNSS solutions become temporarily unavailable wheel odometry maintains the state estimate, albeit with a rapidly increasing estimate uncertainty. This increase in uncertainty is actually desirable as it ensures that the eventually reacquired GNSS solution will not be rejected by the estimator's disturbance rejection threshold which is proportional to the estimate covariance.

GNSS $\rightarrow$ MCL

A transition from GNSS to MCL is detected when the average carrier noise of all satellites drops below the threshold $CN_{0_{lim}}$. Empirical evaluation has shown that for outdoor transitions and outdoor to indoor transitions value of 150-165 indicates a transition. More complete characterization of the threshold metric is left for future work. If this threshold is reached and the error between the current pose estimate and MCL estimated pose is large, then the MCL filter is reinitialized with the current best state estimate. This pose error metric ensures that the filter is not repeatedly reinitialized after GNSS coverage is lost and MCL has started producing the state estimate.

If the MCL filter is mistakenly reinitialized, and a transition has not occurred the algorithm will continue to accept both GNSS and MCL estimates. Without an

information rich map the MCL estimate will degrade and its data will be rejected by the Mahalanobis distance threshold.

MCL

Once initialized and given an information rich map, MCL will produce a low variance pose estimate that will dominate the EKF filter estimate. If errant GNSS solutions are received during this time, they will be rejected as disturbances by the Mahalanbois threshold and ignored. If they are not rejected, the large covariance of the low quality SPP or SPP-SBAS solution (Tab. 4.1) means that the filter effectively ignores them, in favor of the high confidence low variance MCL pose estimate.

MCL $\rightarrow$ GNSS

Transitioning from MCL to GNSS cannot be initiated in the same way as a GNSS to MCL transition. The reason for this is that the system is dependent on the re-acquisition of a high quality GNSS solution, something which is out of the platforms control, unlike the initialization of a map. As the mapped area is exited the MCL solution correction degrades, wheel odometry dominates the estimate, and the state covariance increases. This increase is beneficial because it ensures that when a high-quality GNSS signal is reacquired it will not be rejected as a disturbance by the Mahalanbois threshold.

After the required number of satellites have been brought into view a solution can be calculated and used for localization. Initially these measurements can be noisy and rejected by the rejection threshold, but practice has shown them to converge

rapidly. Once reacquired GNSS can be used to localize in large open, feature sparse areas.

4.5 ROS Implementation

The framework described above has been implemented on a Clearpath Husky running Ubuntu 18.04 LTS and ROS Melodic as summarized in 3. In addition to generic utility nodes, three algorithm implementation nodes are responsible for implementing hybrid localization.

ekf_se_map: The *robot_localization* package [59] provides an EKF sensor fusion node which we use to generate the *map* to *odom* transform. This transform localizes us within the world frame. It takes as measurement input the on-board wheel odometry, MCL generated pose, and GNSS generated 2D position.

It provides an extensible EKF framework and can include as many kinematic sensors as are available. Special care to not include duplicate state measurements has to be taken to prevent filter jitter. Hybrid localization's management of two competing MCL and GNSS pose measurements ensures this does not happen.

navsat_transform: The *robot_localization* package also provides a GNSS coordinate transformation node. It is responsible for translating lat/long solutions into a coordinate frame consistent with a local datum and east-north-up right handed frame. Conversion of the lat/long into an (x,y) point in a local frame allows direct comparison of GNSS with the other measurement modalities. Standard ROS implementations of the node initialize the datum at the location of the first GNSS solution.

Our application requires that coordinates are consistent across deployment cycles and therefore we take advantage of a static datum initialized at the same location every time.

amcl: The ROS *amcl* package [52] provides an adaptive MCL implementation that tracks the 2D pose of a robot against a provided map. A laser scan, map, and odometry transformation matrix are required node topic inputs. This adaptive particle filter measures the approximation error introduced by the discrete representation with the Kullback-Leibler distance. As the approximation error increases more samples are added and vice versa, which has been shown to reduce computational overhead and accelerate convergence.

4.6 Hybrid Localization Results

Testing of the hybrid localization framework presented here was performed both on a university campus and a separate research facility with infrastructure analogous to an industrial facility. Shown here is an example test from the University of Texas campus (Fig **??** The platform has successfully localized itself in both environments and autonomously executed navigation and planning. For the results presented in this work, the mobile platform was teleoperated through environments known to require a hybrid approach for localization. odometry, LIDAR, and GNSS messages were recorded. This data was then fed to the hybrid localization nodes and to determine their efficacy.

The qualitative comparison of four different localization modalities is seen in Fig. 4.3. Raw odometry tracks the route but suffers from continual drift and some

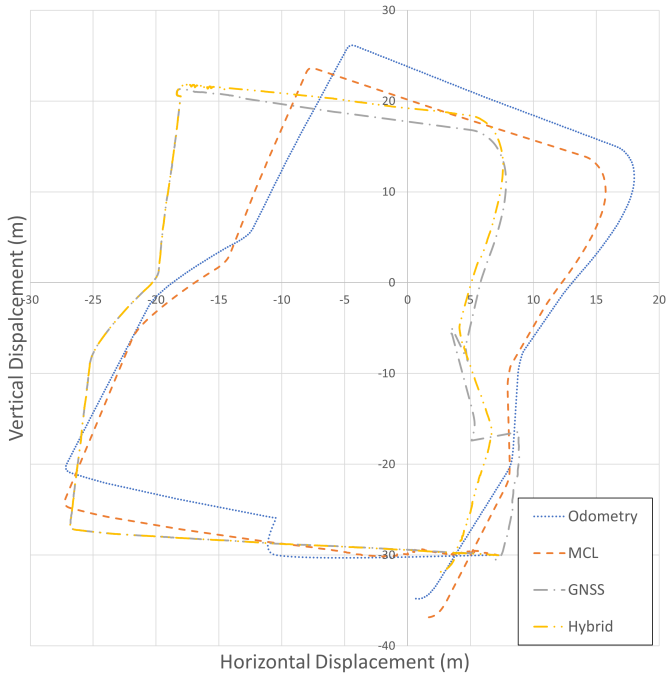

Figure 4.3: State estimate considering all four localization paradigm. Robot traveled clockwise starting and ending in the lower right hand corner

measurement discontinuity. The platform was started in a poorly mapped area which means the MCL estimate relied almost entirely on odometry prediction and closely mimics the raw odometry track. Its continuity and smoothness is a function of the EKF's disturbance rejection which discarded the majority of the incoming MCL pose estimates.

GNSS generated a consistent and accurate estimate in the first half of the course where satellite coverage was robust. However adjacent to large overhead field of view obstruction the receiver was unable to calculate a solution and the estimate. Depending on odometry only, the system significantly deviated from the actual state.

Before the platform fully passed the obstruction, the receiver reacquired a noisy and inaccurate solution which, resulted in jittery and discontinuous behavior of the pose estimate.

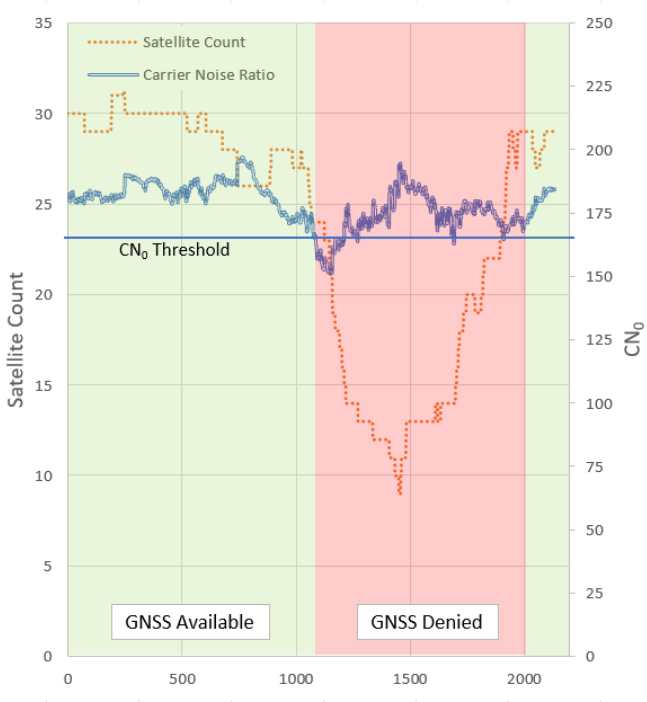

Figure 4.4: Carrier noise ratio and satellite count as a function of time. Note the CN_0 threshold and its rapid response to solution loss.

The developed Hybrid localization generated the most accurate measurements, rejected disturbances, and both autonomously and smoothly transitioned between localization modalities depending on availability. Re-initialization of the MCL filter was triggered by the reduction in the carrier noise ratio below the threshold value (Fig. 4.4). The CN_0 responds more quickly than satellite count when obstructions block the overhead field of view resulting in more timely re-initialization. Another benefit

of CN_0 is that it is calculated for each solution individually. This is in contrast to the covariance of the GNSS estimate which depends on its time history and therefore generates a lagged signal quality metric.

Note that an imperfect *map_mcl* $\rightarrow$ *map* transform, acquired before testing, skewed the final position of the robot. For future deployments it will be possible to improve, validate, and register the needed transform.

Chapter 5

Gas Source Localization

Given a known but randomly selected source location $(x_s, y_s, z_s)_i$ and emission rate q_i, these data can be used to parameterize and evaluate the predicted pollutant concentration $C(\underline{x}) = h(\underline{x})$ at any location $\underline{x}$ in the state space, where $h(\cdot)$ is the GP transport model.

Given a concentration measurement, the likelihood that the predicted pollutant concentration $C(\underline{x})$ was generated by the known but random source can be evaluated. Our particle filter algorithm uses this prediction, measurement, and likelihood evaluation cycle to generate an estimate of the source state

5.1 Setup

Measurements of pollutant concentration c_k are collected across the 3D investigation space at $(x, y, z)_k$. Concurrently a platform mounted meteorological station captures environmental wind speed v_k and azimuth θ_k. These n_k independently generated data are time synchronized with a ROS message synchronizer and fed directly into the filter running on the onboard computer.

Gaussian Plume: General time-dependent 3D concentration gradient of a substance

dispersed by diffusion and advection is described by the *advection-diffusion* equation,

$$\frac{\partial C}{\partial t} = -\vec{\nabla} \cdot (\vec{u}C) + \vec{\nabla} \cdot (D\vec{\nabla}C) + P \tag{5.1}$$

The first term represents the concentrating effect of advection, the second the dispersing effect of diffusion, and the last is the source term. Solution of the full differential equation for the general case is computationally expensive and difficult to accurately model. For the special limiting case of a static solution and the following conditions,

1. Source emission rate is constant and positive
2. Emission are produced from a single stationary source
3. Dispersion is strictly a deterministic function of downwind distance
4. Advection velocity is constant and only in the horizontal 2D plane
5. Workspace is 2D and emissions cannot permeate through the ground surface

These conditions, while applicable for long term time averaged plume modeling, do not accurately capture short term plume emission behavior. Which can result in over predicted downwind concentration or an inaccurate source location azimuth in addition to other complications. The downwind concentration can be predicted with the given GP model as,

$$C(\tilde{\underline{\mathrm{x}}}) = \frac{q}{u} \frac{1}{2\pi\sigma_y\sigma_z} \exp\left(-\frac{\tilde{y}^2}{2\sigma_y^2}\right) \exp\left(-\frac{\tilde{z}^2}{2\sigma_z^2}\right) \tag{5.2}$$

Where coordinates denoted with a *tilde* are represented in a right handed source local frame with its origin at the source location and positive x-axis in the same direction as the wind azimuth. The vertical and horizontal dispersion parameters σ_y and σ_z, functions only of downwind distance, are given by,

$$\sigma_{y,z}(\tilde{x}) = a_{y,z}\tilde{x}(1 + b_{y,z}\tilde{x})^{-c_{y,z}} \tag{5.3}$$

Parameters a, b, c are the static wind parametrization which describe the relative effect of advection and diffusion in the horizontal and vertical planes. These are specified based on the wind parameterization stability class.

Measurement: Pollutant concentration measurements z_k corrupted by zero mean independent and identically distributed Gaussian noise ω_k are collected across the task space.

$$z_k = C_k + \omega_k \tag{5.4}$$

Associated with each of the n_k concentration measurements is a 3D globally referenced coordinate $(x, y, z)_k$. Measurement models are dependent on the sensing modality and sensor errors. Furthermore, data screening can be applied to reduce the variability inherent in gas concentration measurements. This work considers the most general cases of instantaneous real value measurements.

Likelihood Function: Rearranging (5.4) considering that $\omega \sim \mathcal{N}(0, \sigma^2)$, the probability distribution function of the measurement can be written as,

$$p(z_k;\underline{\theta}) = \frac{1}{\sqrt{2\pi\sigma^2}} e^{-\frac{(z_k - C_k)^2}{2\sigma^2}} \tag{5.5}$$

On the right, the exponential error term calculates the difference between the measured concentration z_k, a random variable, and the predicted concentration C_k. The relationship $p(z_k;\underline{\theta})$ represents the probability of the measurement given a deterministic source parameter $\underline{\theta}$. When the predicted concentration and the measured concentration are the same the likelihood is maximized. Considering the entire set of Z^k measurements, the likelihood function is defined as,

$$\Lambda_{Z^k}(\underline{\theta}) \triangleq p(Z^k;\underline{\theta}) \tag{5.6}$$

This likelihood notation is structured to show that the data Z^k has already been acquired, and that it is the parameter set $\underline{\theta}$ that most likely produced the observed data set, which is extracted from the measurement history with a Bayesian filter.

5.2 Particle Filter

Belief in state is represented by a probability density function. As measurement data is collected across the workspace the belief is updated based the new information. Noise corrupted measurements and processes require that statistical estimation techniques like particle filtering be applied. These have the benefit of providing an estimate of the most likely value and a measure of confidence in that estimate.

A Gaussian transformed by a nonlinear function, like the GP model is no longer Gaussian. We consider here the application of nonlinear statistical techniques whose formulation is not dependent on the Gaussian probability density model assumption. Particle filtering is one such technique that represents belief in state by discrete particle approximations. This discrete particle approximation allows for the analytical evaluation of the forward model and the distribution's moments.

Initialization: An area of investigation, for example the area of the industrial facility being surveyed is randomly seeded with np state vectors $\underline{\theta}_j$ drawn from a uniform distribution over the state space, each representing a potential source. This initial set of particles p represents the discrete *a priori* belief in state. Associated with each state is a weight ω_j that quantifies the relative belief that the particle represents the true state. The state vector and its associated weighting is grouped into an individual unit $p_j = [x_s \; y_s \; z_s \; q \; \omega]_j$ called a particle. As the number of particles tends to infinity the discrete probability approximation approaches the true distribution exactly.

Reweight: Each new concentration measurement provides information about the true state. A particle which more closely represents the state that generated the measurement will be weighted more heavily. A weight update for each particle is calculated based on the similarity between the predicted concentration $C(\underline{\theta}_j)$ produced by the source the particle represents and the measured value z_j.

$$w_j(i) = w_j(i-1) \cdot \mathcal{N}_{z_j,\sigma^2}(C(\underline{\theta}_j)) \tag{5.7}$$

To ensure that the particle set represents a axiomatic probability distribution

a normalization such that $\sum_{j=1}^{np} w_j = 1$ is performed. Log-likelihood normalization is used to prevent numerical underflow on precision limited computers.

$$w_j(i) \leftarrow log(w_j(i)) + log(\mathcal{N}_{z_j,\sigma^2}(C(\underline{\theta}_j)))$$
$$w_j(i) \leftarrow exp(w_j(i)) - max(w(i))$$
$$w_j(i) \leftarrow w_j(i)/sum(w(i))$$

Resample: Areas of the state space that contain the true source state should contain more samples. Resampling is the process that places particles in areas of high probability, increasing resolution, and removes particles from areas of low probability.

When the number of effective particles np_{eff} falls below a predetermined threshold np_{min} the resampling algorithm is executed. Effective particle count is used to quantify the number of particles whose weight is sufficiently low that they no longer contribute to the probability belief. If the weight is equally distributed among all np particles then $np_{eff} = np$ and it the weight is carried by one single particle then $np_{eff} = 1$.

The well established multinomial method in Alg. 3 at line 12 implements the resampling step. Particles are chosen from the particle set using a uniform random distribution across the particle cumulative weight sum. A sample with a higher weight is more likely to be replicated.

Algorithm 3 GSL Particle Filter

Initialize np particles p
Load measurements Z^k

for $i = 2 : n_z$ **do**
  $C(\theta_j) = h(\theta_j)$ {Predict}
  $w_j(i) = w_j(i-1) \cdot \mathcal{N}_{z_j,\sigma^2}(C(\underline{\theta}_j))$ {Reweight}
  $w_j = w_j / \sum_{j=1}^{np} w_j \;\; \forall . j$ {Normalize}
  $neff = 1 / \sum_{j=1}^{np} w_j^2$ {Calculate effective particles}

  if $neff < np_{min}$ **then**
    Initialize particle set p_{new}
    for $j = 1 : np$ **do** {Resample}
      $\eta = \mathcal{U}_{[0,1]}(j)$ {Pick}
      Find m such that $\sum_{l=1}^{m-1} w_l \leq \eta < \sum_{t=1}^{m} w_t$
      $p_{new}(j) = p(m)$ with $w_{new} = \frac{1}{np}$
    end for
    $p = p_{new}$
  end if
end for

5.3 Simulated Test Environment

All the hardware components necessary to evaluate the system have assembled and integrated with the mobile platforms and data from each sensor is available in ROS. Due to travel and other restrictions related to the Corona Virus pandemic, we were not able to complete hardware testing for this report, and the effort is scheduled to be completed in the near future.

However, a ROS integrated mobile robotic olfaction simulator GADEN [58] allowed a preliminary evaluation of our gas source localization implementation.

GADEN breaks simulation into three steps:

1. Environment Definition
2. Wind Simulation
3. Gas Dispersion Simulation

Environment Definition

The environment consists of the 3D structures that interrupt or modify fluid flow. GADEN allows the construction of these environments using publicly or commercially available computer automated design programs. Two 3D polymesh descriptions of the environment, describing the internal and external structure, are exported and taken as input for the wind simulation step.

Wind Simulation

GADEN uses the open source computational fluid dynamics (CFD) tool OpenFoam [12] to simulate the wind velocity in each discretized cell. OpenFOAM uses the 3D polymesh generated in the environment definition step as input. The complexity of CFD modeling is a challenge for non-expert users therefore accepted generic parameterizations of the model and solver for non-compressible air flow are used with the GADEN package. Simulated wind flow patterns, either static or dynamic, are exported from OpenFOAM for use in the gas filament dispersion simulator.

Gas Dispersion Simulator

Integrating the filament model from [31] into a ROS package is the most significant contribution of the GADEN package. The filament model previously discussed is run offline with the output of the environmental model and CFD simulation. Its output, describing the filament dispersion, is stored in configuration files and then replayed for simulation. In addition to simulating the filament model the package provides ROS integrated simulated gas and anemometer sensors.

5.4 Results

Presented here is the results of a test of our particle filter gas source localization algorithm in the GADEN olfaction simulator.

Simulated Environment

In Fig. 5.1 the simulated environmental is shown. On the left hand side the RGB axis represents the origin of the map frame that pose estimates are made with respect to. To the right of the RGB axis a green rectangular bollard that represents the gas source. Emanating from the top of the gas source are black particles representing the emitted filaments. On the right side of the figure the blue body is the environmental sensing platform, containing both a simulated anemometer and gas sensor. The green arrow represents the simulated anemometer measured azimuth.

The GADEN filament model is paramaterized in a launch file and evaluated before run time and stored for replay during simulation. A variable rate of between zero and ten filaments released are released each second. Each filament has an emis-

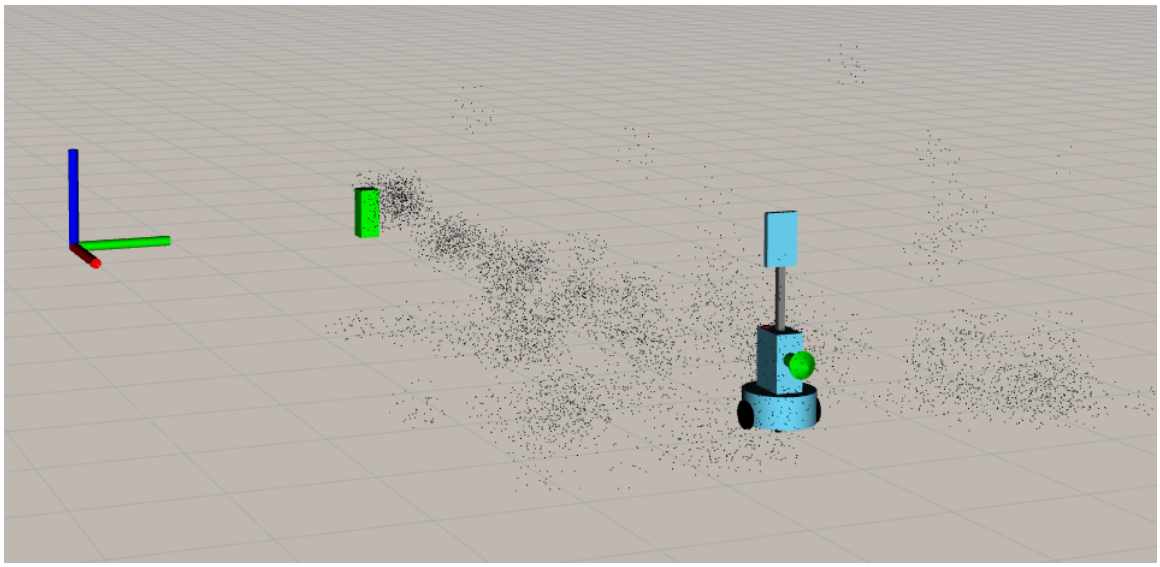

Figure 5.1: Simulated GADEN olfaction gas source emission environment in RVIZ.

sion concentration of 10ppm at its center and an initial standard deviation of 10cm. Each filament is disturbed by turbulent eddies as it is transported by advection. The filament standard deviation growth ratio is $10\frac{cm^2}{s}$ and sampled white noise with a standard deviation of 2cm is added at each simulation time step.

A sample of the measured gas concentration is shown in Fig. 5.2 given as ppm with respect to time. It is readily apparent that modeling the measurement signature is challenging. Even when downwind of the source, total measurement blackouts occur for extended periods of time. Controlled field tests and experience with emission modeling on short time scales has shown the intermittent character of concentration measurements to be a major complicating factor. A known limitation of the GP model is that it explicitly assume concentration is invariant with respect to time.

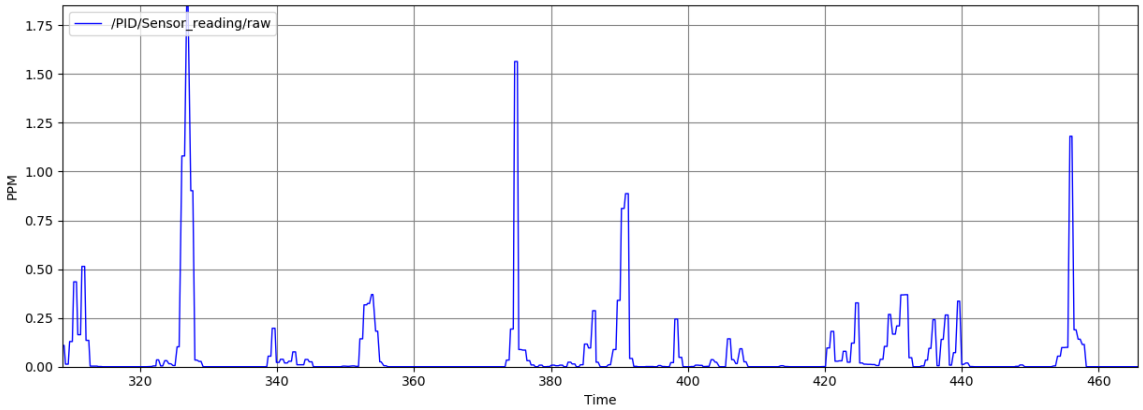

Figure 5.2: Measured gas concentration in the GADEN simulator. The sporadic noisy measurement replicates conditions described in controlled field tests.

Anemometer measurements from GADEN are shown in Fig. 5.3. The cell velocity calculated during the pre-processing wind simulation step is taken at the anemometer location in the map frame. Samples from a Gaussian distribution are then drawn and used to corrupt the simulated wind cell velocity. This corrupted measurement is then published to ROS by the simulated anemometer node. Our gas source localization particle filter node subscribes to this topic and receives the simulated measurement. It is used to parameterize the forward transport model to evaluate the likelihood function for each particle.

As measurements are taken and processed by the filter, information is extracted from them. This information is used to update our probability distribution which represents our belief about the true source state. Without an informative prior our filter initializes the state space with a uniform distribution of particles. This is represented in Fig. 5.4 by the random initial spread of the particles represented by red cylinders. As time progresses and measurements are taken, the particle filter is

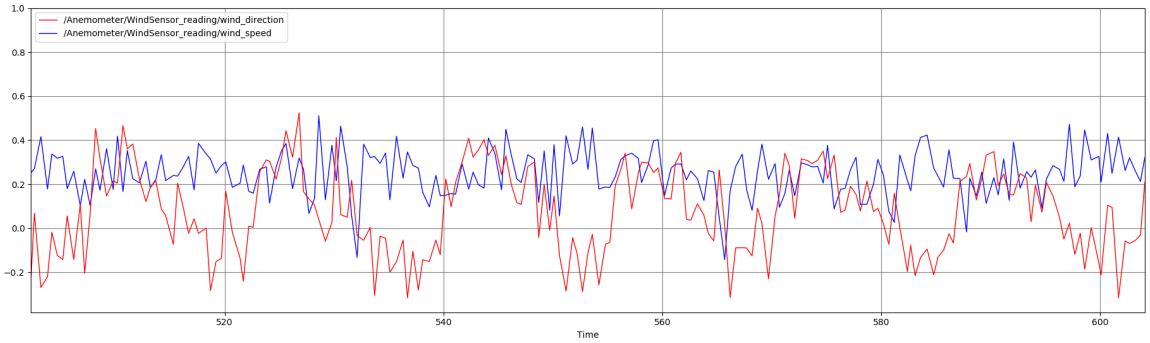

Figure 5.3: Measured wind direction (red) in radian and speed (blue) in m/s measured by the simulated anemometer in the GADEN simulation environment.

evaluated continuously. Particles in unlikely portions of the state space are eliminated and areas with a high likelihood are populated with more particles. In Fig. 5.5 the filter state is shown mid-convergence after partial information has been extracted from the measurement stream. Quantifying time to convergence is challenging because of uncertainty around the state space size, measurement information value, and noise model. Shown in Fig. 5.6 is the filter state after convergence. The particles, themselves each representing a simulated source, have converged to approximately the same location as the simulated source represented by the green bollard.

The convergence of the filter's pose estimate is shown in Fig. 5.7 where the blue

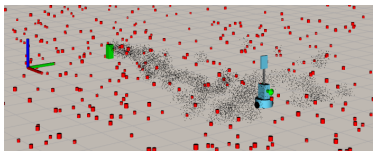

Figure 5.4: Particles immediately after initialization

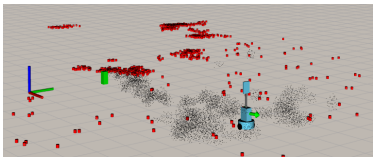

Figure 5.5: Particles converging to the true source location

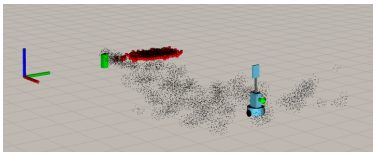

Figure 5.6: Particle converged near the true state

data represent the filters most likely belief at each update and the orange dot is the simulated true state. Immediately after initialization, the most likely filter estimate, is the center of the state space over which the uniform distribution is sampled over, the coordinate (0,0) in this experiment. The particle set covariance at initialization is infinity. Given facility maps, or an *a priori* assessment of likely emission sources, an informative prior can be used to reduce convergence time and the likelihood of a spurious source estimates.

On startup the information available in each measurement is relatively large compared to the information encoded in the particle set. Therefore the first 10-20 measurement evaluations cause large updates to the particle set when resampled. During this initial convergence, before the probability density is well structured by the likelihood function, the estimate can temporarily diverge from the true state. Before particles have been culled from unlikely areas the likelihood of many of the particles will be low and contribute little to the effective particle count. Resampling happens often when the first informative measurements are received because the number of effective particles after each reweighting is likely to be below the threshold.

Convergence to the true state cannot be guaranteed because of the stochastic nature of the filament dispersion model and inaccuracy in the assumptions behind the GP model. Our results visualized in Fig. 5.8 show the filter building an informed prior on the source location from noisy and discrete environmental measurements. This prior can then be given to plant operators who can locate and then eliminate the emission source. After the particle set has converged to a pointed likelihood distribution, updates happen less frequently and the incremental change in the most

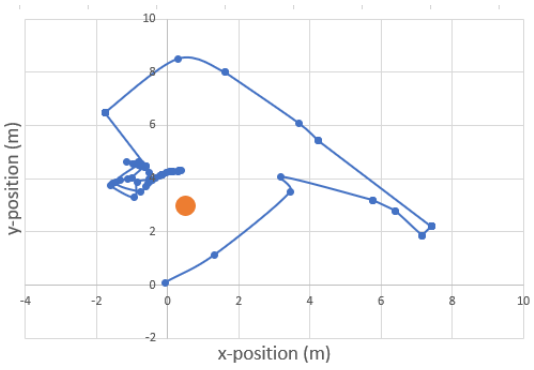

Figure 5.7: Most likely state estimate (blue) and the true state (orange). Initial resampling causes large updates in belief when compared to later measurements which only produce small incremental updates after the filter has converged.

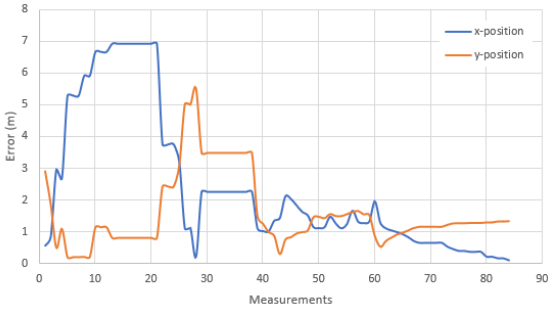

Figure 5.8: Error between the most likely estimate and the true state as a function of resampling measurement steps for the two linear dimensions. The measurement device was for this test was static and therefore the horizontal resolution (y-position) performed worse than the vertical.

likely estimate goes to zero. The peakedness of the likelihood function derived from the GP model is dependent on the coordinate direction and wind parameterization. This likelihood anisotropy results in a 1m error in the y-position and less than 0.1m of error in the x-position. In real deployments the motion of the robot horizontally across the plume increases horizontal resolution and decreases horizontal position error.

5.5 Roadmap for Hardware Testing

As stated at the beginning of the chapter, the Corona Virus prevented development and testing of the localization model on hardware. Both gas and anemometer sensors have been integrated with the Philbart platform in hardware and software. The particle filter has also been integrated in ROS to be compatible with the pub-

lished environmental sensor message types. Testing at the University of Texas is planned for Spring 2021. A controlled CO2 release will serve as a surrogate for a fugitive emission leak and the gas sensing hardware on the platform will be adjusted to measure CO2 instead of methane.

Chapter 6

Conclusion and Future Work

6.1 Conclusion

Modern robotic platforms in downstream O&G facilities have the potential to enhance safety and efficiency. This effort focused on addressing to capabilities that are necessary for robust deployment and added value in industrial environments: robust navigation and fugitive emission detection and localization.

6.1.1 Philbart

Previously deployed platforms like the MIMROex, Sensabot, and Argonaut underwent rigorous hazardous environmental certification. Considering however that the role these platforms will play in facilities is not proven, the expense in time and money to certify platforms may not be justified. There are a broad range of analog industrial facilities without hazardous atmospheres that can be used to validate the application of remote operators. Since these systems show there is a path for certification, reserving the certification process for after a capability has been proven will encourage the testing and deployment of robots in O&G facilities.

This work, although interrupted by the 2020 Corona Virus pandemic, demonstrates that uncertified platforms can deploy and validate remote operator capabili-

ties. Large industrial companies are risk averse and plan for piece-wise integration of new technology. Furthermore capital expenditure on large technology programs happen over long time scales which means it is important that the use case is validated up front. Our use of commercial off the shelf hardware and open source software meant that the platform could be developed rapidly and use case proven with significantly less up front engineering than other efforts.

6.1.2 Hybrid Localization

Maintaining an accurate pose estimate of Philbart is critical for all remote operator tasks. This is an active and broad area of research and technical application. Localization solution complexity varies widely, from single use run time algorithms to complex full area map reconstruction. The refinery environment and practical limitations on technology solutions available to field operations are important considerations. Also the limited availability of signals that can used for localization is unique to large industrial processing facilities.

Our hybrid localization strategy takes advantage of the complementary availability of GNSS and LIDAR localization solutions, and accuracy of inexpensive GNSS and LIDAR sensors. Collecting and maintaining accurate full facility maps for MCL algorithms is not feasible. Nor is complete GNSS satellite coverage available in refinery facilities. Our solution is to separate the workspace into areas of preferred sensing modalities and arbitrate the transition between them. Maintaining an accurate pose estimate across challenging sensing occluded environments allows for long term autonomy and minimum operator input or supervision during deployment.

6.1.3 Gas Source Localization

Sensor networks in oil & gas facilities are designed to detect explosive or poisonous gas levels. They are prone to false alarm and cannot localize an emission source except by its proximity to the sensor. The environmental sensing package and gas source localization algorithm deployed on Philbart augments facility operators ability to detect emissions. When an alarm is triggered the platform can automatically deploy to the area of concern to verify the conditions the alarm indicates actually exist. Older facilities with outdated sensor networks frequently experience false alarms which require valuable facility operator time and effort to rectify.

Mobile robot gas source localization, instead of mimicking a previously performed task, is a new capability introduced by our platform to the downstream space. The ability of mobile robot platforms with gas and anemometer sensors to localize emission sources has been proven in laboratory and field setting but not in real industrial facilities. Our algorithm when deployed has the potential to augment the operator with a new capability that will increase safety and allow for the elimination of fugitive emissions.

6.2 Future Work

Robotic platforms in industrial facilities are proliferating across the globe. Development of a well equipped mobile platform, capable of guaranteeing localization for long term autonomy, and providing accurate gas source localization algorithms is only part of a diverse technical field. While this work explored these three ideas there is exciting work still to be done.

6.2.1 Robotic Platforms in Downstream Facilities

Deploying Philbart into an decommissioned analog downstream oil & gas processing facility will allow for the field validation of our proposed method. As previously stated the 2020 Corona Virus pandemic prevented a field deployment in time for the conclusion of this thesis. As more and more companies begin to explore robotic operator augmentation we believe that uncertified commercial off the shelf platforms will be the best tool for proof of concept applications.

Ongoing efforts to integrate a manipulator mounted camera with the mobile base are being explored (Fig. 6.1). Automated visual inspection of valves, gauges, and sight glasses though not originally in the project scope is an area of great interest to facility operators. As the set of tasks which that can be automated increases, the demand for the platform increases. When an as yet undiscovered viability threshold is met the urgency to deploy platforms like Philbart will grow.

6.2.2 Hybrid Localization

The relationship between carrier noise and GNSS solution availability is known to exist and is used as a transition metric in our hybrid localization algorithm. Our experiments however do not fully elucidate this relationship or assign causality to its behavior in commonly encountered environments. Testing and recording the metric response across a variety of sensor occlusion scenarios will provide the information required to accurately assess the transition metric threshold. With a better understanding of the threshold and its dependence on environment our hybrid localization algorithm can more accurately predict transitions. Furthermore it is possible that the

Figure 6.1: A HEBI manipulator with attached GoPro mounted on the Philbart mobile base.

metric trend before total loss of the GNSS solution could provide advanced warning about predicted transitions.

6.2.3 Gas Source Localization

Sensing modalities including infrared cameras and spectroscopy-based remote lasers are increasingly deployed on mobile robotic platforms. Recent work developed informative search strategies for a platform mounted with such a spectroscopy-based remote gas sensor [53] in an indoor environment. The ability to sense emissions

remotely allows for increased state space coverage and for increased stand off between the platform and the hazardous environment. Actively classifying hazardous atmosphere zone in real time using remote emission sensors has the potential to significantly decrease the risk profile associated with mobile robots. If developed further remote sensing has the potential to influence how electrical systems including active robotic sensing platforms are allowed to operate in O&G facilities.

Our source localization algorithm likelihood models a single emission source. Multi-source emission scenarios are challenging to model because in our deployment context the number of source cannot be explicitly known *a priori*. Reversible jump MCMC methods [34] hare used to dynamically adjust the size of the state space such that the state model better explains the observed phenomenon. Sampling based methods like particle filters do however suffer from the curse of dimensionality and increases in state space size can tax computer hardware. Building and demonstrating an adaptive state space gas source localization Bayesian filter in a refinery environment would be a valuable contribution.

Bibliography

[1] Argonaut. https://www.theengineer.co.uk/unmanned-platforms-offshore-automation/. Accessed: 2020-11-24.

[2] Directive 2014/34/eu of the european parliament and of the council. https://eur-lex.europa.eu/legal-content/EN/TXT/PDF/?uri=CELEX:32014L0034&from=EN.

[3] Exrobotics. https://exrobotics.global/. Accessed: 2020-12-03.

[4] Filament dispersion model. https://cse.final-year-projects.in/wp-content/uploads/2018/03/p-03531-A-3D-Gas-Dispersion-Simulator-2.jpg. Accessed: 2020-11-27.

[5] Gaussian plume. https://image.slidesharecdn.com/11airpollutiondispersion-140930114022-phpapp02/95/11-air-pollution-dispersion-14-638.jpg?cb=1412077280. Accessed: 2020-11-27.

[6] Gill sonic anemometer. https://www.omniinstruments.co.uk/gmx200-weather-station.html. Accessed: 2020-11-23.

[7] Husky mobile base. https://www.unmannedsystemstechnology.com/wp-content/uploads/2014/01/Husky-Ground-Robot.png. Accessed: 2020-11-28.

[8] Iecex standards documentation. https://www.iecex.com/publications/standards/.

[9] Intel realsense d435. https://www.adorama.com/images/Large/in82635kprq.jpg. Accessed: 2020-11-22.

[10] Microstrain imu. https://www.microstrain.com/sites/default/files/styles/product_thumb/public/gx5-25-whitebg.jpg?itok=e9LL2ac. Accessed: 2020-11-23.

[11] Mimroex. https://www.researchgate.net/figure/Fraunhofer-MIMROex-robot-inspecting-a-process-plant-during-field-test-on-the-topside-of_fig1_266209662. Accessed: 2020-11-24.

[12] Openfoam. https://www.openfoam.com/. Accessed: 2020-11-17.

[13] Refinery. https://www.freepik.com/premium-photo/oil-refinery-petrochemical-plant-with-cooling-tower_3800447.html. Accessed: 2020-11-22.

[14] Rki m2a methane sensor. https://www.instrumart.com/assets/M2A-360.jpg?width=660&height=495&scale=upscalecanvas&bgcolor=fff. Accessed: 2020-11-22.

[15] Ros node and topic graph. https://answers.ros.org/upfiles/15026035891055113.png. Accessed: 2020-11-29.

[16] Sensabot. https://www.nrec.ri.cmu.edu/media/success-story-pages/shell-deploys-sensabot.html. Accessed: 2020-11-24.

[17] Sick tim 571 lidar. https://www.neffpower.com/ecomm_images/items/thumb/1079742.png. Accessed: 2020-11-22.

[18] Swiftnav duro. https://www.cbj.ca/swift. Accessed: 2020-11-22.

[19] Ultrasonic depth camera. Accessed: 2020-12-01.

[20] Ut austin pma plaza. https://www.google.com/maps/@30.2885725,-97.7363186,97m/data=!3m1!1e3. Accessed: 2020-10-01.

[21] Zed stereo depth camera. https://www.stereolabs.com/zed/. Accessed: 2020-12-01.

[22] A gps and laser-based localization for urban and non-urban outdoor environments. pages 149–154. IEEE, 2008.

[23] Air quality dispersion modeling - preferred and recommended models. *EPA*, Nov 2020.

[24] Gnss integration in the localization system of an autonomous vehicle based on particle weighting. *IEEE Sensors Journal*, 20(6):3314–3323, 2020.

[25] Javier M Antelis and Javier Minguez. Eeg source localization based on dynamic bayesian estimation techniques. page 6.

[26] W. Baetz, A. Kroll, and G. Bonow. Mobile robots with active ir-optical sensing for remote gas detection and source localization. In *2009 IEEE International Conference on Robotics and Automation*, pages 2773–2778, 2009.

[27] M Bengel, K Pfeiffer, B Graf, A Bubeck, and A Verl. Mobile robots for offshore inspection and manipulation. In *2009 IEEE/RSJ International Conference on Intelligent Robots and Systems*, pages 3317–3322. IEEE, 2009.

[28] G. Blewitt. Basics of the gps technique: Observation equations. 1997.

[29] C.P.-A. Bourque and P.A. Arp. Simulating sulfur dioxide plume dispersion and subsequent deposition downwind from a stationary point source: A model. *Environmental Pollution*, 91(3):363–380, 1996.

[30] Angelo Coluccia and Alessio Fascista. A review of advanced localization techniques for crowdsensing wireless sensor networks. *Sensors*, 19(5):988, Feb 2019.

[31] Jay A Farrell, John Murlis, Xuezhu Long, Wei Li, and Ring T Cardé. Filament-based atmospheric dispersion model to achieve short time-scale structure of odor plumes. *Environmental fluid mechanics (Dordrecht, Netherlands : 2001)*, 2(1):143–169, 2002.

[32] Yanbin Gao, Shifei Liu, Mohamed Atia, and Aboelmagd Noureldin. Ins/gps/lidar integrated navigation system for urban and indoor environments using hybrid scan matching algorithm. *Sensors*, 15, 09 2015.

[33] P. Goel, S. I. Roumeliotis, and G. S. Sukhatme. Robust localization using relative and absolute position estimates. In *Proceedings 1999 IEEE/RSJ International Conference on Intelligent Robots and Systems. Human and Environment Friendly Robots with High Intelligence and Emotional Quotients (Cat. No.99CH36289)*, volume 2, pages 1134–1140 vol.2, 1999.

[34] PETER J GREEN. Reversible jump markov chain monte carlo computation and bayesian model determination. *Biometrika*, 82(4):711–732, 1995.

[35] A Gunatilaka, B Ristic, A Skvortsov, and M Morelande. Parameter estimation of a continuous chemical plume source. In *2008 11th International Conference on Information Fusion*, pages 1–8. IEEE, 2008.

[36] Sue Ellen Haupt. A demonstration of coupled receptor/dispersion modeling with a genetic algorithm. *Atmospheric environment (1994)*, 39(37):7181–7189, 2005.

[37] Bin He, Toshimitsu Musha, Yoshiwo Okamoto, Saburo Homma, Yoshio Nakajima, and Toshio Sato. Electric dipole tracing in the brain by means of the boundary element method and its accuracy. *IEEE Transactions on Biomedical Engineering*, BME-34(6):406–414, Jun 1987.

[38] Heesung Chae, Christiand, Sunglok Choi, Wonpil Yu, and Jaeil Cho. Autonomous navigation of mobile robot based on dgps/ins sensor fusion by ekf in semi-outdoor structured environment. In *2010 IEEE/RSJ International Conference on Intelligent Robots and Systems*, pages 1222–1227, 2010.

[39] Bamdad Hosseini and John M. Stockie. Bayesian estimation of airborne fugitive emissions using a gaussian plume model. *Atmospheric Environment*, 141:122–138, Sep 2016. arXiv: 1602.09053.

[40] James W Howse, Lawrence O Ticknor, and Kenneth R Muske. Least squares estimation techniques for position tracking of radioactive sources. page 11, 2001.

[41] Michael Hutchinson, Hyondong Oh, and Wen-Hua Chen. A review of source term estimation methods for atmospheric dispersion events using static or mobile

sensors. *Information Fusion*, 36:130–148, 2017.

[42] H Ishida, K Suetsugu, T Nakamoto, and T Moriizumi. Study of autonomous mobile sensing system for localization of odor source using gas sensors and anemometric sensors. *Sensors and actuators. A. Physical.*, 45(2):153–157, 1994.

[43] G Johannesson, B Hanley, and J Nitao. Dynamic bayesian models via monte carlo - an introduction with examples -.

[44] R. E. Kalman. A new approach to linear filtering and prediction problems. *ASME Journal of Basic Engineering*, 1960.

[45] Andrew Keats, Eugene Yee, and Fue-Sang Lien. Bayesian inference for source determination with applications to a complex urban environment. *Atmospheric environment (1994)*, 41(3):465–479, 2007.

[46] S. Kohlbrecher and O.v. Stryk. From robocup rescue to supervised autonomous mobile robots for remote inspection of industrial plants. In *Künstl Intell*. Springer, 2016.

[47] K. Kydd, S. Macrez, and P. Pourcel. Autonomous robot for gas and oil sites. Society of Petroleum Engineers, 20015.

[48] Sheldon Landsberger, Mitch Pryor, Derek Haas, Unmil Karadkar, and James Sulzer. Development of mobile platform for inventory and inspection applications in nuclear environments. page 203.

[49] James Lents, Michael Walsh, Kebin He, Nicole Davis, Mauricio Osses, Sebastian Tolvett, and Huan Liu. *Handbook of Air Quality Management*. Bantam, 1988. `http://www.aqbook.org/`(visited 2020-11-03).

[50] Jesse Levinson, Michael Montemerlo, and Sebastian Thrun. Map-based precision vehicle localization in urban environments. 2007.

[51] Ji-Gong Li, Qing-Hao Meng, Yang Wang, and Ming Zeng. Odor source localization using a mobile robot in outdoor airflow environments with a particle filter algorithm. *Autonomous robots*, 30(3):281–292, 2011.

[52] David Lu and Michael Ferguson. robot_localization, 2011.

[53] Arain MA, Hernandez Bennetts V, Schaffernicht E, and Lilienthal AJ. Sniffing out fugitive methane emissions: autonomous remote gas inspection with a mobile robot. *The International Journal of Robotics Research*, 2020.

[54] L Marques, N Almeida, and A.T de Almeida. Olfactory sensory system for odour-plume tracking and localization. In *Proceedings of IEEE Sensors 2003 (IEEE Cat. No.03CH37498)*, volume 1, pages 418–423 Vol.1. IEEE, 2003.

[55] L Marques and A.T De Almeida. Electronic nose-based odour source localization. In *6th International Workshop on Advanced Motion Control. Proceedings (Cat. No.00TH8494)*, pages 36–40. IEEE, 2000.

[56] Wim Meeussen. Coordinate frames for mobile platforms. btxdoc.pdf, October 2010.

[57] D.R Middleton, J.D Butler, and D.M Colwill. Gaussian plume dispersion model applicable to a complex motorway interchange. *Atmospheric Environment (1967)*, 13(7):1039–1049, Jan 1979.

[58] Javier Monroy, Victor Hernandez-Bennetts, Han Fan, Achim Lilienthal, and Javier Gonzalez-Jimenez. Gaden: A 3d gas dispersion simulator for mobile robot olfaction in realistic environments. *MDPI Sensors*, 17(7: 1479):1–16, 2017.

[59] Tom Moore and Daniel Stouch. robot_localization, 2014.

[60] Patrick P Neumann, Victor Hernandez Bennetts, Achim J Lilienthal, Matthias Bartholmai, and Jochen H Schiller. Gas source localization with a micro-drone using bio-inspired and particle filter-based algorithms. *Advanced robotics*, 27(9):725–738, 2013.

[61] F. Pasquill. The estimation of the dispersion of windborne material. pages 33–40, 1961.

[62] I. Peerless, A. Serblowski, and B. Mulder. A robot that removes operators from extreme environments. Society of Petroleum Engineers, 20016.

[63] Kay I. Penny. Appropriate critical values when testing for a single multivariate outlier by using the mahalanobis distance. *Journal of the Royal Statistical Society: Series C (Applied Statistics)*, 45(1):73, 1996.

[64] N. Schmitz, J. Koch, M. Proetzsch, and K. Berns. Fault-tolerant 3d localization for outdoor vehicles. In *Proc. IEEE/RSJ International Conference on Intel-*

ligent Robots and Systems (IROS'06), pages 941–946, Beijing, China, October 2006.

[65] Inanc Senocak, Nicolas W. Hengartner, Margaret B. Short, and W. Brent Daniel. Stochastic event reconstruction of atmospheric contaminant dispersion using bayesian inference. *Atmospheric Environment*, 42(33):7718 – 7727, 2008.

[66] Ehab M. Shaheen and Sherif A. Elgamel. Mathematical analyses of the gps receiver interference tolerance and mean time to loss lock. *Defence Technology*, 15(3):440 – 449, 2019.

[67] R. Thrapp, C. Westbrook, and D. Subramanian. Robust localization algorithms for an autonomous campus tour guide. In *Proc. IEEE International Conference on Robotics and Automation (ICRA'01)*, pages 2065–2071, Seoul, Korea, May 2001.

[68] Sebastian Thrun, Wolfram Burgard, and Dieter Fox. *Probabilistic Robotics (Intelligent Robotics and Autonomous Agents)*. The MIT Press, 2005.

[69] G. Trehard, E. Pollard, B. Bradai, and F. Nashashibi. On line mapping and global positioning for autonomous driving in urban environment based on evidential slam. In *2015 IEEE Intelligent Vehicles Symposium (IV)*, pages 814–819, 2015.

[70] D.B. Turner. *Workbook of Atmospheric Dispersion Estimates*. Government Printing Office, Washington, D.C. 20402, 1969.

[71] P. Urcola, M. T. Lorente, J. L. Villarroel, and L. Montano. Seamless indoor-outdoor robust localization for robots. In Manuel A. Armada, Alberto Sanfeliu, and Manuel Ferre, editors, *ROBOT2013: First Iberian Robotics Conference*, pages 275–287, Cham, 2014. Springer International Publishing.

[72] R. W. Wolcott and R. M. Eustice. Visual localization within lidar maps for automated urban driving. In *2014 IEEE/RSJ International Conference on Intelligent Robots and Systems*, pages 176–183, 2014.

[73] Eugene Yee. Bayesian probabilistic approach for inverse source determination from limited and noisy chemical or biological sensor concentration measurements. In Augustus W. Fountain III, editor, *Chemical and Biological Sensing VIII*, volume 6554, pages 255 – 266. International Society for Optics and Photonics, SPIE, 2007.

[74] W. Zhang and J. Kosecka. Image based localization in urban environments. In *Third International Symposium on 3D Data Processing, Visualization, and Transmission (3DPVT'06)*, pages 33–40, 2006.

[75] Xiaoping Zheng and Zengqiang Chen. Back-calculation of the strength and location of hazardous materials releases using the pattern search method. *Journal of hazardous materials*, 183(1):474–481, 2010.